

Aus der
Klinik für Orthopädie und Unfallchirurgie
Klinik der Universität München
Direktoren: Prof. Dr. Wolfgang Böcker und Prof. Dr. Boris Holzapfel

**Fusion of Normoxic- and
Hypoxic-Preconditioned Myoblasts
Leads to Increased Hypertrophy**

Dissertation
zum Erwerb des Doktorgrades der Medizin
an der Medizinischen Fakultät
der Ludwig-Maximilians-Universität zu München

vorgelegt von
Tamara Pircher

aus
Meran

Jahr
2025

Mit Genehmigung der Medizinischen Fakultät
der Universität München

Berichterstatter: Prof. Dr. Wolfgang Böcker
Mitberichterstatter: Prof. Dr. Claudia Veigel
Prof. Dr. Benedikt Schoser

Mitbetreuung durch den
promovierten Mitarbeiter: Dr. Maximilian Saller

Dekan: Prof. Dr. med. Thomas Gudermann

Tag der mündlichen Prüfung: 13.03.2025

Abstract

Interruptions in blood supply due to diseases or traumas lead to ischemic muscle injury. The most common causes are arterial embolism, prolonged arterial clamping during trauma or vessel damage, acute atherosclerotic thrombosis and critical limb ischemia caused by atherosclerotic plaques. Further reasons are chronic diseases such as chronic obstructive pulmonary disease and heart failure, which cause muscle atrophy and weakness through prolonged hypoxemia. Within trauma centers, the morbidity is closely associated with ischemia, often resulting in residual disability or even amputation. Hence, a deeper understanding of skeletal muscle regeneration and the effect of oxygen depletion is crucial to identify and develop new therapies that support skeletal muscle survival. Prior *in vitro* studies only analyzed skeletal muscle regeneration at fixed oxygen partial pressures, whereas this thesis aimed to observe more practical conditions, as oxygen concentration is more variable in real-life considerations.

During regeneration, myoblasts are exposed to higher or lower oxygen local concentrations, depending on the vascular function around the muscle cells. Currently, the impact of variations in partial pressure of oxygen on myoblast proliferation and differentiation, as well as the interplay between oxygen-treated myoblasts during the differentiation process, is not well known. This thesis explored the relationship between hypoxic conditioned (2% O₂, C2C12^{RFP}) and standardized ("normoxic", 21% O₂, C2C12^{GFP}) cultured myoblasts within two different saturated environments. The effects of hypoxia on myoblast morphology, number and area of myotube formation and myotube size were investigated. For a more detailed analyses between both myoblast groups and for visual differentiation, the coding sequences for different fluorescent proteins were stably introduced. Therefore the newly fused myotubes (MT) could be divided in three subpopulations (MT^{GFP}, MT^{RFP}, MT^{GFP+RFP}), depending on the merged myoblasts.

Results showed a downregulation of the total number of myotubes, when hypoxic

and normoxic-conditioned myoblasts were seeded together, regardless of the oxygen concentration during differentiation. Despite their decrease in number, a hypertrophic response of cells within the normoxic environment was observed. Interestingly, the analysis of the transcriptome by RNA sequencing revealed various gene expressions known for hypoxic adjustment of cancer cells. Therefore, this thesis hypothesizes a similar metabolic reprogramming strategy between the myotubes and cancer cells. However, further loss- and gain-of-function experiments on the potential candidate genes are needed for validation.

Zusammenfassung

Der einheitliche Pathomechanismus von Ischämien der Skelettmuskulatur ist eine inadäquate Sauerstoffversorgung der Muskulatur. Dabei kann es sich sowohl um eine traumatische Ursache, wie eine Gefäßverletzung, als auch um einen nicht-traumatischen Auslöser, wie beispielsweise arterielle Embolien, akute arteriosklerotische Thrombosen oder kritische Extremitätenembolien, meist durch arteriosklerotische Plaques hervorgerufen, handeln. Zudem kommen chronische Erkrankungen wie etwa die chronisch obstruktive Lungenerkrankung (COPD) und die Herzinsuffizienz als mögliche Ursachen einer Skelettmuskelischämie in Frage. Da die Morbidität zumeist in Traumazentren stark vom Ausmaß der Ischämien abhängt, bedarf es eines besseren Verständnisses der Regenerationsprozesse, sowie der Auswirkungen von Hypoxie auf die Skelettmuskulatur, um neue Therapieansätze zur Verhinderung von Gewebsverlust zu entwickeln.

Es wurden bereits mehrere *In-Vitro*-Studien zur behandelten Thematik durchgeführt, wobei die Muskelregeneration stets unter konstantem Sauerstoffpartialdruck beobachtet wurde. Da die Sauerstoffkonzentration im Gewebe bei praxisnaher Betrachtung einer großen Variation unterliegt, sollte die vorliegende Studie realistischere Bedingungen voraussetzen, indem die Regeneration unter verschiedenen Sauerstoffkonzentrationen beobachtet wurden. Um die Auswirkung des Sauerstoffgehaltes auf die Morphologie der Myoblasten zu erfassen, bediente man sich zweier unterschiedlicher Gruppen derselben. Die eine, versetzt in Hypoxie (2% O₂, C2C12^{RFP}) und die andere unter Standardbedingungen ("Normoxie", 21% O₂, C2C12^{GFP}). Anschließend sollte zunächst eine Interaktion zwischen den beiden Gruppen während der Differenzierung beobachtet werden. Dabei waren vor allem die Anzahl, Größe und die Fläche der neu formierten Myotuben zur genaueren Betrachtung relevant.

Um die verschiedenen Myoblastengruppen während der Analysen voneinander unterscheiden zu können, wurden fluoreszierende Proteine zur Färbung injiziert. Nach

erfolgreicher Differenzierung ergaben sich daraus drei Untergruppen aus neu formierten Myotuben (MT^{GFP} , MT^{RFP} , $MT^{GFR+RFP}$). Durch die entstandenen Mischfärbungen wurde analysiert, welche Zellen sich verbunden hatten.

Obwohl sich durch die Fusion der unterschiedlich kultivierten Myoblasten eine Verringerung der Gesamtzahl an Myotuben zeigte, wurde gleichzeitig eine Hypertrophie der Myotuben im Vergleich zur "Reingruppe" beobachtet. Dabei ist es wahrscheinlich, dass die Myoblasten einem ähnlichen Reprogrammierungsschema folgen wie Tumorzellen unter hypoxischen Bedingungen. Diese Annahme beruht auf die in dieser Studie identifizierten Gene, welche im Rahmen der hypoxischen Anpassung exprimiert wurden. Selbige Gene konnte in vorangegangenen Studien bei der hypoxischen Anpassung von Tumorzellen beobachtet werden. Die genauere Betrachtung der aussichtsreichsten Sequenzen bildet die Grundlage für zukünftige Studien.

Contents

Abstract	I
Zusammenfassung	III
Contents	V
1 Introduction	1
1.1 Influence of hypoxia on skeletal muscle development, maintenance and regeneration	2
1.2 Self-renewal of skeletal muscle cells within hypoxia	3
1.2.1 NOTCH signaling pathway	4
1.2.2 Non-canonical Wnt signal transduction pathway (WNT) signalling pathway	4
1.2.3 CDKN1A/B (p21/p27)	5
1.3 Skeletal muscle cell proliferation within hypoxia	6
1.3.1 Erythropoietin	6
1.3.2 Negative Feedback-Loop of proliferation	7
1.3.3 PI3K-AKT-mTOR signaling pathway	7
1.3.4 Histone deacetylases	8
1.4 Skeletal muscle cell differentiation within hypoxia	9
1.4.1 Epigenetic regulation	9
1.4.2 Hypoxia inducible factor 1 and 2 alpha (HIF1A/HIF2A)	10
1.4.2.1 Negative-loop regulation of HIF1A	12
2 Aim of the study	13
3 Materials & Methods	15
3.1 Cell lines	15

3.2	Transfection with coding sequences for fluorescence proteins	16
3.3	Morphological changes	18
3.4	Population doubling and population doubling time	19
3.5	Myoblast fusion assay	19
3.6	Analysis of the relative number of myotubes	20
3.7	Analysis of the relative myotube area	22
3.8	mRNA-isolation and sequencing	23
3.9	Bioinformatic analyses	24
3.10	Statistical analysis	24
4	Results	25
4.1	Prolonged hypoxic exposure affects the morphology of C2C12 myoblasts but does not change their proliferation	25
4.2	<i>In vitro</i> myoblast fusion is inhibited by long-term hypoxia	26
4.3	Novel myoblast fusion assay used to analyze interaction of normoxic and hypoxic conditioned myoblasts	27
4.4	Myogenic differentiation of normoxic and hypoxic preconditioned my- oblasts is affected by abrupt changes of oxygen concentrations	28
4.5	Fusion of hypoxic with normoxic conditioned myoblasts results in larger myotubes	29
4.6	Oxygen Tension Differentially Influences Cell Fusion among Different Precultured Cell Populations	32
4.7	Hypoxia Leads to Delayed Expression of Genes Encoding Regulators of Myogenic Differentiation	32
5	Discussion	43
5.1	Long-Term Hypoxia Has No Significant Impact on Myoblast Morphology or Proliferation but Leads to Reduced Myogenesis	44
5.2	Hypoxia Leads to Increased Synergy between Hypoxia- and Normoxia- Cultured Myoblasts	45
5.3	Hypoxic Transcriptional Changes Are Partially Reversible during Myo- genic Differentiation	46
5.4	Within Hypoxia, Skeletal Muscle Hypertrophy Shows Parallels to Cancer Cell Behavior	51

6 Outlook	53
Bibliography	54
List of Abbreviations	75
List of Figures	80
List of Tables	81
List of Equations	82
Publications	83
Eidesstattliche Versicherung	84
Acknowledgements	85
Erklärung zur Übereinstimmung	86

Chapter 1

Introduction

The human body consists of over 600 individual muscles, each serving a diversity of functions including blood circulation, movement execution and support, weight lifting and childbirth. All muscles can be classified into three types - cardiac, smooth and skeletal muscles. They serve different muscular functions through contraction or relaxation both under conscious or unconscious control. This thesis focuses on the skeletal muscle, composed of bundles of striated myofibers, enveloped by a basal lamina and formed by a highly organized cytoskeleton.

The skeletal muscle originates from the paraxial mesoderm. This transient tissue is divided into a posterior and anterior region. Within the latter, somites are formed and the skeletal myogenesis is initiated (1). After their formation, somites are compartmentalized into a dorsal epithelial dermomyotome, the origin of muscle progenitor cell (MPC), and a ventral mesenchymal sclerotome, deriving to the axial skeleton and tendons, bones and cartilage, respectively (1). The following myogenesis is divided into two phases: the first phase produces primary slow-switching myofibers deriving from $PAX3^{+}/PAX7^{+}$ dermomyotomal progenitors (2, 3) and the second phase resulting in secondary fast-switching myofibers due to the fusion of the primary myofibers (4, 1).

During secondary myogenesis, *paired-box transcription factor 3* ($PAX3$) is downregulated and expansion of muscle mass is sustained by cell fusion and the addition of myonuclei from proliferating *paired-box transcription factor 7* ($PAX7$)⁺ progenitors (1). A subset of the $PAX7^{+}$ cells form a quiescent, adult stem cell pool, the so-called satellite cell (SC) (5). During advancing myogenesis, a few promising signalling molecules have been described. The hepatocyte growth factor (HGF), essential for proper my-

oblast migration (6), WNT-signalling, promoting their fusion (7) and fibroblast growth factor (FGF), acting on proliferation, through simultaneous inhibition of their differentiation process (8, 9).

After birth, the stem cell pool is diminished only by a few percentages of the multinucleated cells in adult muscle and it turned out to be highly dependent on NOTCH signalling (10).

1.1 Influence of hypoxia on skeletal muscle development, maintenance and regeneration

For metabolic signalling, energy production and cellular homeostasis within skeletal muscle tissue, oxygen (O_2) is a crucial factor. While the atmospheric oxygen concentration maintains approximately 21%, the physiological level within skeletal muscle tissue varies between 2%-10% depending on their location within the body (11). Oxygen deprivation within skeletal muscle at a reduced level below 2% (12) is called hypoxia. This condition either occurs physiologically (during embryogenesis, at high altitude adjustment and exercise stimuli) or is caused by pathologies. The main hypoxia-associated diseases are traumatic muscle injuries or vessel destruction, acute atherosclerotic thrombosis and critical limb ischemia due to peripheral arterial disease (PAD) (13).

Within embryogenesis, some MPCs (muscle progenitor cells) remain quiescent and localized between the sarcolemma and the basal membrane: the satellite cells (SCs). They correspond to resident stem cells, which can be activated during regeneration processes or hypertrophy in adult skeletal muscle. Furthermore, they are characterized by their PAX7 expression (14). During development and skeletal muscle regeneration, the SCs are frequently exposed to hypoxic niches, which have been shown to be critical for SC activation, self-renewal, proliferation and differentiation (15). Once SCs are activated and begin to differentiate towards myoblasts, they express the further myogenic regulatory transcription factor (MRF)s: *myogenic differentiation 1* (*MYOD1*) and *myogenic factor 5* (*Myf5*) (7). According to the expressed markers, three different cell-types can be distinguished: $PAX7^+/MYOD1^-$ (quiescent and self-renewing SC), $PAX7^+/MYOD1^+$ (activated, proliferating SC-derived myoblasts) and $PAX7^-/MYOD1^+/Myogenin^+$ (myoblasts that differentiate into multinuclear myotubes)

(16).

The adult skeletal muscle regeneration is subdivided in three phases: The destruction and inflammatory phase (Phase 1), the repair phase (Phase 2) and finally the maturation phase (Phase 3) (17). Damaged myofibers control the migration of SCs into the injury site through WNT7a signalling (18) after SCs activation and expression of *MYOD1*. Within phase two and three, skeletal muscle regeneration resembles the differentiation program of embryogenic myogenesis (19). The following newly formed myotubes are characterized by their expression of *myosin heavy chain (MYH)*, similar to newly formed myotubes during embryogenesis (20).

1.2 Self-renewal of skeletal muscle cells within hypoxia

To increase stem cells and simultaneously preserve the stem cell pool throughout life, the mechanism of self-renewal is necessary. Self-renewal depends on different gene expressions and signaling pathways described in the following paragraph.

MiRNAs (microRNAs) are post-transcriptional regulators and can be impacted by reactive oxygen species (ROS), as well as by modifications in the oxygen level (21). Thus far, eight microRNA (miRNA)s are known to be specific for a muscle tissue and to be involved in myogenic processes. These heart- and skeletal muscle-specific miRNAs are named myomiRs and include *miR1*, *miR206*, *miR133A/B*, *miR208A/B*, *miR486*, *miR499* (22), *miR26A* (23) and *miR210* (21). Among them, *miR206* is the sole regulator exclusively expressed in skeletal muscles (24). Together with *miR1*, *miR206* is activated by MYOD1 and targets *PAX3* and *PAX7* mRNA (22).

In normoxia ($> 2\% \text{ O}_2$), small non-coding miRNAs as *miR1* & *miR206* lead to down-regulation of the PAX7 protein by recognition of the 3'UTR of the mouse *PAX7* mRNA (25, 26). Therewith, hypoxia reduces *miR1* & *miR206* expression, allowing *PAX7* to regulate the asymmetric self-renewal division of satellite cells. This ensures a sufficient large stem cell pool, while not affecting the overall proliferation (16). *MiR1* and *miR133* are suggested to be required for proper somatogenesis (27), while changes in *miR208b* and *miR499* expression during muscle atrophy are involved in plasticity (28). Finally, *miR210* is known as vascular endothelial growth factor (VEGF) target, ensuring myotube survival during mitochondrial dysfunction or oxidative stress. It modifies mitochondrial metabolism via the modulation of ROS regeneration and direct repression

of gene expression that are related to apoptosis, such as *CASP8-associated protein 2 (CASP8AP2)* (29) (Fig. 1.1).

1.2.1 NOTCH signaling pathway

The main responsible signalling pathways for self-renewal process are the NOTCH and non-canonical WNT signalling cascades (Fig. 1.1). The NOTCH signalling pathway is active during embryogenic muscle development, promoting cell division. Furthermore, NOTCH is highly expressed throughout the regeneration of hypoxic associated muscle injuries. NOTCH leads to an upregulation of *hes related family bHLH transcription factor with YRPW motif 2 (HEY2)*, which itself results in a downregulation of myogenic differentiation. In addition, this maintains the undifferentiated state of the myogenic cells (30). Acute hypoxia leads to an interaction between the forkhead box O1 transcription factor (FOXO1) and to the NOTCH pathway, itself leading to the upregulation of downstream transcription factor genes *hes family bHLH transcription factor 1 (Hes1)* and *hes related family bHLH transcription factor with YRPW motif 1 (Hey1)* (31). The latter ones suppress *miR1* and *miR206* in a MyoD1-independent manner to prevent proliferation (16) (Fig. 1.1).

1.2.2 Non-canonical WNT signalling pathway

WNT signalling can be either canonical or non-canonical and both pathways are important regulators of myogenesis (32, 33). While the canonical WNT pathway mainly mediates SC division, the non-canonical WNT cascade is involved during skeletal muscle hypertrophy through asymmetric expansion of SC and myofiber growth. The non-canonical WNT has a notable impact within hypoxia (34). In these conditions, non-canonical WNT signalling can be activated by two different mechanisms: the protein kinase C (PKC), which activates calcium/calmodulin-dependent protein kinase II (CAMKII) and the Ras homolog family member A/c-Jun N-terminal kinases (RHOA/JNK) pathways, which lead to activating transcription factors/ cAMP response element binding protein (ATF/CREB) activation (35). Essential proteins of the non-canonical pathways are Wnt7, Wnt9a and Wnt4 (36). Especially, the upregulation of *Wnt4* has been shown to increase *myogenin (MYOG)* expression (37), which is necessary for differentiation (Fig. 1.1).

1.2.3 CDKN1A/B (p21/p27)

In order to differentiate, it is necessary for cells to withdraw from the cell cycle, which is regulated by cyclin-dependent kinase (CDK)s and their inhibitors (cyclin-dependent kinase inhibitors (CDKI)s). In severe hypoxia ($<1\% \text{ O}_2$), cyclin-dependent kinase inhibitor 1A (CDKN1A) (also known as p21), a major target of the tumor suppressor p53 (TP53), is inhibited (38). Physiologically, it regulates the cell cycle progression by the inhibition of cyclin/CDK complexes (38) and leads to the accumulation of the tumor suppressor protein retinoblastoma (RB) (38). This is necessary to establish a permanent post-mitotic state in myogenesis (39, 40) (Fig. 1.1).

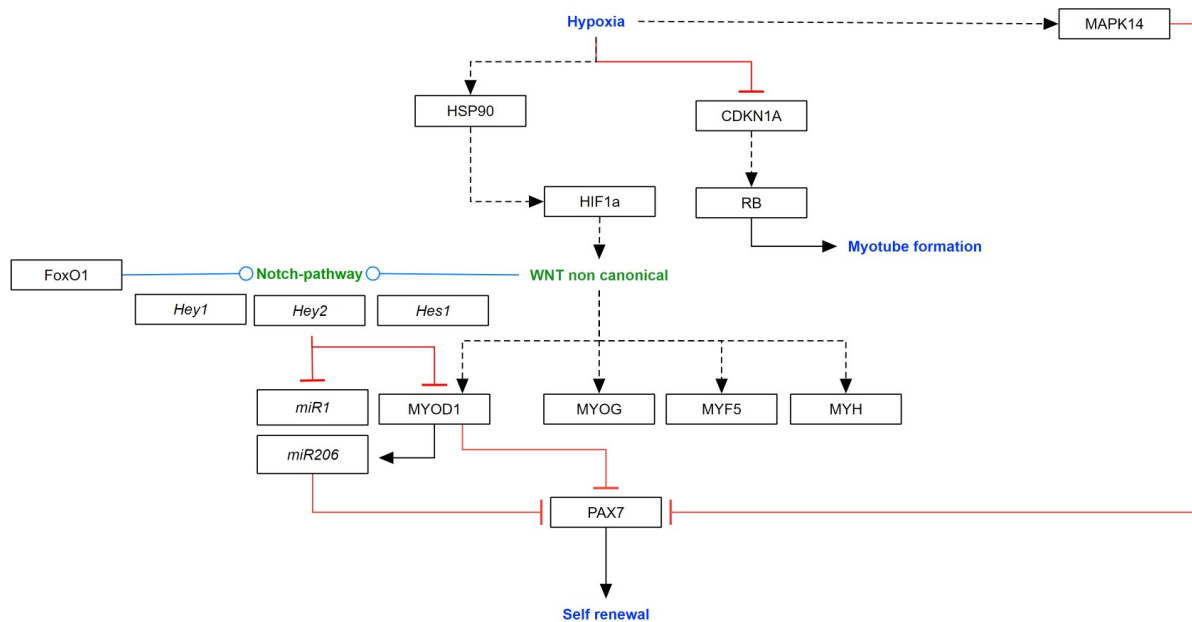


Figure 1.1: Molecular mechanisms involved in self-renewal of satellite cells in hypoxia. Black arrows: activation of the signalling pathway / protein / molecule. Blunt red arrow: inhibition of the signalling pathway / protein / molecule. Round blue arrow: interaction between two pathways. Adopted and modified from Pircher et al. (41).

1.3 Skeletal muscle cell proliferation within hypoxia

The rapid growth and reproduction of new cells is called proliferation. For skeletal muscle cells, the proliferation includes division of the myoblasts, in order to increase their number. The cell proliferation is driven from different factors, including hormones and growth factors. Within hypoxia, some of the known proliferation mechanisms within skeletal muscle cells are changed or different from the known processes at "normal" conditions.

In previous studies, an oxygen level of 2% has shown to stimulate mouse satellite cells (42) and human primary myoblasts (43) proliferation *in vitro*. During proliferation *MYOD1* and *Myf5* are the prominent MRFs and remain highly expressed until late differentiation. In contrast, *MYOG* and *myogenic factor 6 (MYF6)* dominate as regulatory transcription factors during differentiation(44, 45, 46).

1.3.1 Erythropoietin

During hypoxia, the hormone erythropoietin (EPO) (induced by lack of oxygen) is released by the kidney to stimulate red blood cell production. Recent observations showed an additional effect on C2C12 and primary satellite cells. EPO stimulates proliferation and inhibits differentiation by the induction of *MyoD1* and *Myf5* (47). Further data also indicated an increase of SC survival in skeletal muscle due to endogenous EPO (48).

Thereby, EPO stimulates the recruitment and proliferation of SC in injured muscle and increases phosphatidylinositol 3 kinase (PI3K)-protein kinase B (AKT)-associated proteins (48). In addition, it has been shown that upregulated EPO induces GATA3 expression, a transcription factor increased during C2C12 proliferation. It enables the activation of Janus kinase 2 / signal transducer and activator of transcription 5A (JAK2/STAT5a) pathways (48), which are upregulated during early myogenic differentiation *in vitro* (49) (Fig. 1.2). Similar results were shown by the hypoxia-regulated heme oxygenase 1 (HMOX1), by increasing the expression of *MyoD1* and *MyoG* under ischaemic conditions (50, 51).

1.3.2 Negative Feedback-Loop of proliferation

Physiologically, MYOD1 translation is regulated by AKT, preventing MYOD1 degradation in a F-box protein 32 (FBXO32)- and tripartite motif containing 63 (TRIM63)- dependent manner during proliferation (52). In hypoxia, AKT signalling is inhibited, which subsequently leads to MYOD1 degeneration (53). The responsible mechanism is a negative feedback-loop during proliferation: myoblasts release the transforming growth factor- β superfamily member *myostatin* (*MSTN*) (54), leading to decreased MYOD1 expression. Thereby MSTN binds to activin receptor type-2B (ActRIIb) and activates SMAD family member 2 (SMAD2) (53). MSTN was described as oxygen-dependent key molecule in regulation of myogenesis (55). Hypoxia interferes in this negative loop mechanisms by causing myoblasts to release MSTN (56). As a result, proliferation is downregulated (54). Additionally, it has been reported, that MSTN can be inhibited by calcitriol, independent of the oxygen level (57).

MSTN can additionally activate insulin-like growth factor 2 (IGFII) (57). Due to reduced IGF1 receptor (IGFIR) sensitivity at low oxygen levels, the PI3K-AKT signalling pathway is partially downregulated (58) (Figure 1.2).

1.3.3 PI3K-AKT-mTOR signaling pathway

As described above, the PI3K-AKT-mTOR pathway plays a pivotal role within myogenic proliferation and differentiation (55), due to its prevention of MYOD1 degradation and due to the stimulation of MYOD1 translation via mammalian target of rapamycin (mTOR1) activation. Physiologically, mTOR1 is either activated directly (54) or indirectly by AKT, by the inhibition of tumor-suppressant proteins that form the tuberous sclerosis complex (TSC) (58). TSC regulate the Ras-related small GTPase Ras homolog enriched in brain (RHEB), which in turn adjusts mTOR1 activation (59). Once the skeletal muscle cells are exposed to hypoxia or stress, the AMP-activated protein kinase (AMPK) and DNA-damage-inducible transcript 4 (DDIT4) pathways are activated, leading to a suppression of RHEB and therefore to a downregulation of the indirect mTOR1 activation (60).

Additionally, hypoxia has a direct negative effect on the PI3K-AKT-mTOR pathway (55) (Fig. 1.2).

1.4 Skeletal muscle cell differentiation within hypoxia

After proliferation, the unspecialized (immature) SCs undergo transcriptional adaptation to reach a more specific (mature) function and shape. Thereby, myoblasts are formed to myotubes. Hypoxia seemed to inhibit myoblast differentiation.

Skeletal muscle differentiation is divided into early and late phases, both regulated by different active MRFs. During early differentiation, Myf5 and MYOD1 are expressed. MYOD1 removes cells from the cell cycle and enhances the transcription of MYOG, which together with myogenic regulatory transcription factor 4 (MRF4), dominates the late differentiation phase (62).

Several studies investigated the effect of hypoxia on myogenic differentiation. On one hand, it has been shown that severe hypoxia ($<1\% \text{ O}_2$) leads to decreased RB, CDKN1A, MYOD1, MYOG and myosin heavy chain 1 (MYHC1) and increased cyclin-dependent kinase inhibitor 1B (CDKN1B) (also known as p27) (38). This results in growth arrest and inhibition of the MRFs expression and myogenic differentiation. On the other hand, an upregulation of various MRFs due to hypoxic preconditioning of myogenic cells were shown by Crillo et al (36). A decreased MYOD1 inhibition due to downregulation of inhibitor of differentiation/ DNA binding 1 (ID1) and myogenic repressor (MYOR) was observed (36). During the initialization of the switch from differentiation to proliferation within hypoxia, a decreased mitogen-activated protein kinase family member 14 (MAPK14) is observed (55). Under physiological conditions, MAPK14 (p38) mediates phosphorylation by differentiating myoblasts and is involved in the terminal differentiation of myoblasts by activating MYOD1 and myocyte enhancer factor-2 (MEF2) (55).

1.4.1 Epigenetic regulation

Lysine Demethylase 6A (KDM6A) has recently been discovered to prevent cell differentiation by demethylation of histone H3 on lysine 27 (H3K27) under physiological conditions (63). During hypoxia however, H3K27 methylation and repression of late transcription genes such as *MYOG* have been observed. By deeper investigations, different oxygen affinities between the two subtypes KDM6A and Lysine Demethylase 6B (KDM6B) were detected, suggesting that the hypoxic effect to promote H3K27 methylation results

through a specific loss of KDM6A activity during low oxygen levels.

Therefore, Abhishek et al investigated the difference between both histone demethylases, by comparing the catalytic Jumonji C (JmjC) domains. They found two non-conserved residues M¹¹⁹⁰ (KDM6A) → T¹⁴³⁴ (KDM6B) and E¹³³⁵ (KDM6A) → D¹⁵⁷⁹ (KDM6B). A variant of KDM6A harboring these two KDM6B-like changes showed a 2-fold increased affinity of oxygen *in vivo* and greater rescuing of differentiation under hypoxic conditions compared to the native KDM6A (63).

1.4.2 Hypoxia inducible factor 1 and 2 alpha (HIF1A/HIF2A)

In 2019, the Nobel Prize in Physiology and Medicine, was awarded to the three physician scientists i.e. William G. Kaelin, Jr., Peter Ratcliffe and Gregg Semenza, for their discovery and characterization of Hypoxia-inducible factor 1 (HIF1). They demonstrated direct linkage of gene expression response to oxygen availability and the oxygen levels in animal cells, allowing immediate cellular responses to occur for oxygenation through the action of the HIF1 transcription factor complex.

Hypoxia-inducible factor 1 alpha is the most studied heterodimeric transcriptional regulator of the cellular and developmental response to hypoxia and balances proliferation during hypoxia. At high oxygen concentrations, the ubiquitination and proteasomal degradation of Hypoxia-inducible factor 1 alpha (HIF1A) is catalyzed by prolyl hydroxylase (PHD)(PHD1, PHD2, PHD3). The best known is PHD2, encoded by *EGLN1* (64). Once the oxygen level drops, the alpha-subunit of HIF1A is stabilized by heat shock protein 90 (HSP90) to prevent degradation (65, 66) and translocated to the nucleus, where it forms a heterodimer with its HIF1 beta subunit (HIF1B). The newly formed complexes bind to hypoxia response element (HRE) in the promoter region of target genes, as for example genes involved in blood oxygen capacity (*EPO* or *HMOX1*), proangiogenic genes (*VEGF*, *adrenomedullin (Adm)*) and metabolic genes associated with glycolysis and glucose uptake (65), including *phosphofructokinase (PFK)*, *pyruvate kinase (PK)* and *lactate dehydrogenase (LDH)* (67). *VEGF* has a pro-angiogenetic function (66) and is necessary during skeletal muscle regeneration (68). However, it can also induce stress fiber formation in muscle-specific fibroblasts of dystrophic muscles, leading to fibrosis (69).

An additional target of HIF1A is Class E basic helix-loop-helix protein 40 (BHLHE40),

which participates in the TP53 signalling pathway and can additionally be upregulated by hypoxia itself. BHLHE40 binds to the E-box sequence of the *MYOG* promoter, leading to reduced transcriptional activity of *MYOD1* on *MYOG* (70). Moreover, a direct inhibition of Myf5, MYOD1, MYOG, myogenic regulatory transcription factor 6 (MRF6) and MYH, as well as the canonical WNT signalling pathway (71, 58) due to HIF1A was reported. This leads to a repressed myogenic proliferation and differentiation.

Even though HGF is not a target gene of HIF1A, it is worth a closer look, since it has a special connection with the transcription factor. HGF is known to have a major impact on myogenesis and adult muscle regeneration due to its interaction with the PI3K-AKT-mTOR signalling pathway (70) and CDKN1A (53) and its downregulation in hypoxia. Several studies showed that this effect is caused by a HRE in the promoter region of HGF, which is bound by HIF1A during low oxygen levels (72).

Another important member of the HIF-family is the hypoxia inducible factor 2 alpha (HIF2A), predominantly expressed in quiescent satellite cells. Over 90% of the *PAX7*⁺ satellite cells are HIF2A positive (73), which improves slow myofiber formation. Despite the fact that no HIF1A was detected in *PAX7*⁺ satellite cells, a decreased self-renewal and differentiation of myoblasts within hypoxia without effect on the proliferation was shown. A key indicator was the double knockout of HIF1A and HIF2A in mice. This indicates that both factors are necessary for self-renewal within hypoxia. Regarding physiological conditions, no differences in the muscle stem cells were observed by the knockout (74).

Both hypoxia inducible transcription factors have a pro-angiogenic function within skeletal muscle cells (66).

Contrary to HIF1A, HIF2A acts downstream of peroxisome proliferator-activated receptor- γ coactivator 1a (PGC-1a) (75), in order to enhance the slow myofiber formation, to promote stemness of satellite cells (16, 58) and to directly activate the expression of leukemia inhibitor factor (LIF) in colorectal cancer (76). LIF acts precisely on the site of injury and stimulates hypertrophy (77, 78). However, further research is needed, whether similar LIF expression is stimulated in skeletal muscle regeneration, resulting in a provocation of myoblast growth and fusion *in vivo*.

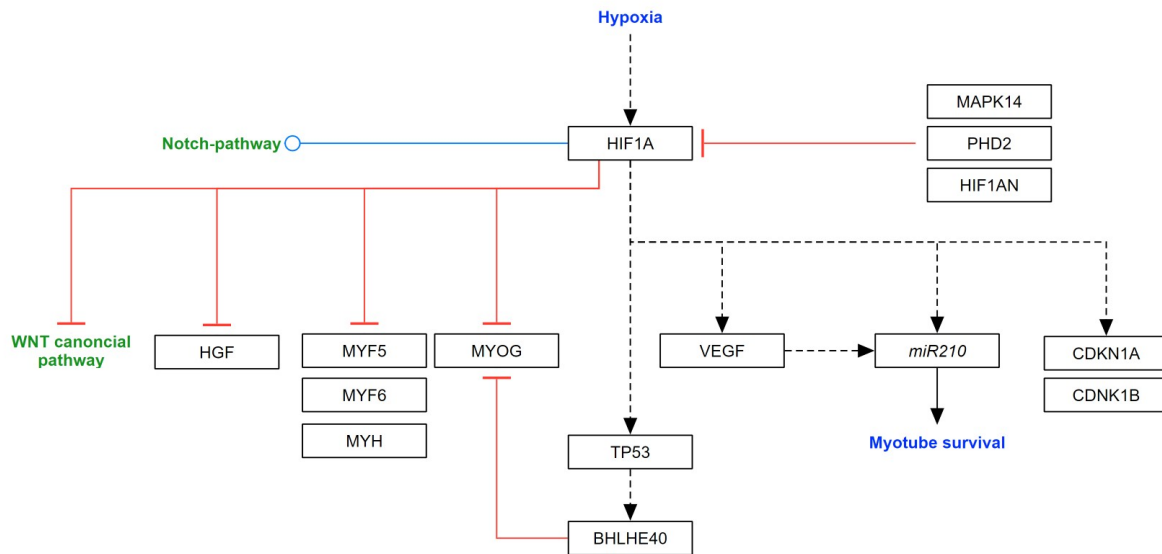


Figure 1.3: HIF1A modulates myogenic differentiation in hypoxia. Black arrow: activation of the signaling pathway/ protein/ molecule. Blunt red arrow: inhibition of the signaling pathway/ protein/ molecule. Round blue arrow: interaction between two pathways. Adopted and modified from Pircher et al. (41).

1.4.2.1 Negative-loop regulation of HIF1A

The key element of the negative-loop regulation of HIF1A is the alpha-ketoglutarate-dependent dioxygenase hypoxia-inducible factor 1-alpha inhibitor (HIF1AN). During hypoxia, it is downregulated in order to allow HIF1A stabilization. But, once the oxygen concentration rises, it hydroxylates the C-terminal transactivation domain of HIF1A (79). Remarkably, the HIF1AN also has a negative impact on the NOTCH signalling pathway, which once more highlights the linkage between HIF1A and NOTCH-pathway (80).

Another already discussed signalling pathway showed to have an effect on the HIF1A downregulation: MAPK14. During hypoxia, MAPK14 is activated by high mobility group protein B1 (HIMGB1), through receptor for advanced glycation end-products (RAGE) (81). Another study reported an impact of estradiol (E2) on MAPK14 phosphorylation and therefore an effect on HIF1A (82) (Fig. 1.3).

Chapter 2

Aim of the study

The survival and proper functioning of aerobic organisms necessitate an oxygen-rich environment. Within the skeletal muscle, various processes including metabolism, embryogenesis and regeneration, cell proliferation and differentiation, as well as intercellular pathways, are susceptible to changes in local and temporal oxygen concentration. Within the musculoskeletal system, skeletal muscle cells have a lower threshold for ischaemic damage (ischaemic tissue time) of around 5 hours, when compared to nerves (ischaemic tissue time: 8 hours), skin (24 hours) or bones (4 days), emphasizing the high impact of oxygen onto this tissue (83). After 6 hours of ischemia, muscles become severely injured, ranging from a loss of muscle function to necrosis (84). Several pathological causes, including arteriosclerosis, peripheral arterial diseases, as well as torn muscle fibers and extreme muscle traumas result to hypoxic conditions within skeletal muscle cells. This can be seen as an epidemiologic problem. While arteriosclerosis is one of the major diseases in adult patients causing critical limb ischemia (13), extreme muscle trauma is the most common injury seen in trauma centers. The morbidity is highly allied to ischemia, often resulting in residual disability or even amputation (85, 86). Once the damage occurred, satellite cells migrate into the injured area and initiate the regenerative process (87, 88). Therefore, a sufficient blood flow and oxygenation is necessary (89).

Increased tolerance to hypoxic damage could enhance preservation of skeletal muscle mass, as it has already been shown within heart muscle. For ischemic heart diseases, it is well established that hypoxic preconditioning can protect cardiomyocytes from cell death during myocardial ischemia (90). Liu et al. started to investigate a

similar therapy method. The transplantation of skeletal muscles with hypoxic conditioned myoblasts yielded a significant increase in satellite cells, thereby demonstrating augmented self-renewal capacity and greater ease of satellite cell compartment occupation *in vivo* (16). Until today, we do not know how oxygen partial pressure variances affect myoblast proliferation and differentiation. Furthermore, we especially do not understand how different oxygen-conditioned myoblast interact among each other during differentiation process. Therefore, the aim of this thesis was the investigation of the interaction between hypoxic conditioned (2% O₂, C2C12^{RFP}) and standardized ("normoxic", 21% O₂, C2C12^{GFP}) cultured myoblasts within two different saturated environments (normoxia: 21% O₂ and hypoxia: 2% O₂). Precisely, the often used 21% O₂ standard level for myoblast incubation does not describe physiological "normoxia" within skeletal muscle cells, but rather a hyperoxia. However, we decided to continue with "normoxia" at 21% O₂.

Main focuses in this thesis were:

- I What is the impact of different oxygen levels on C2C12 cell proliferation and differentiation?
- II Can morphological differences between myoblasts cultured in two different oxygen levels be observed?
- III Can two C2C12 populations, priorly cultured in different oxygen levels fuse under each other? If yes, is there a difference between the different oxygen conditions?
- IV What are the effects of different oxygen levels on the transcriptome of differentiating C2C12 myoblasts?

Chapter 3

Materials & Methods

The Materials and Methods part outlines the theory and techniques utilized to achieve the research objectives and verify the hypotheses proposed in this thesis.

3.1 Cell lines

For each experiment the C2C12 murine immortalized myoblast cell line, an established cell culture model for skeletal muscle development, was used. The C2C12 cells were developed for *in vitro* studies and are mainly utilized in biomedical research for myoblasts proliferation and myogenesis (91) (Figure 3.1).

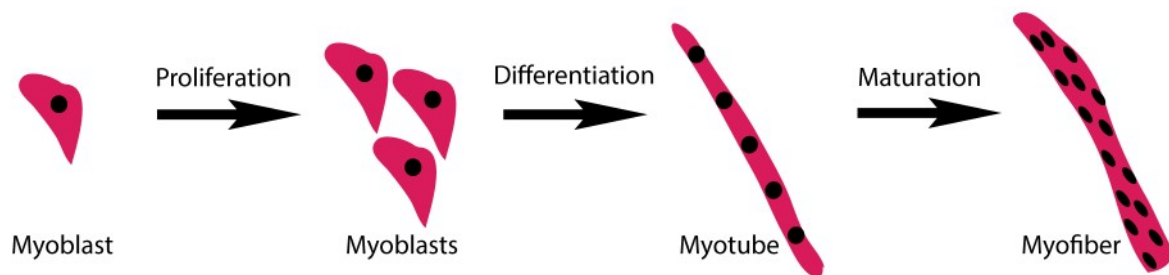


Figure 3.1: C2C12 myoblast model: C2C12 myoblasts proliferate rapidly. When the cells reach a confluence $>50\%$, differentiation is induced. This happens due to cell-to-cell contact. As a result, they start to spontaneously fuse into multinucleated cells (myotubes). Further on, myotubes can mature to myofibers (not visualized in this thesis).

C2C12 mouse myoblasts (Sigma Aldrich, USA) were cultured in growth medium (GM) at 37°C in a $5\% \text{CO}_2$ and 95% humidified atmosphere. The GM

was composed of Dulbecco's Modified Eagle Medium (DMEM) with GlutaMAX I (Thermo Fisher, USA) supplemented with 10% fetal bovine serum (FBS) (Sigma Aldrich, USA) and 40 IU/ml penicillin/streptomycin (Biochrom, Germany). Medium was changed at least twice per week if not stated otherwise. The cell confluence was not allowed to exceed 50% in order to avoid spontaneous fusion of C2C12 cells. At 50%, the cells were passaged. Therefore, they were washed twice with phosphate-buffered saline (PBS) without Ca^{2+} and Mg^{2+} (PAA Laboratories GmbH, Pasching, Austria) and afterwards trypsinized using 4 ml of 0.5 g/l Trypsin (Invitrogen, Karlsruhe, Germany) with 0.2 g/l ethylenediaminetetraacetic acid disodium salt dehydrate (EDTA) (Sigma-Aldrich, St. Louis, MO, USA) dissolved 1:10 in PBS. The culture flasks with the Trypsin were incubated for 5 minutes in a humidified incubator at 5% CO_2 and 37°C until the cells totally detached from the surface. Afterwards, in order to inhibit the enzymatic reaction, GM in combination with a doubled volume of the prior used trypsin was used. To count the detached C2C12 cells, a Neubauer counting chamber was used. In the end, 500'000 C2C12 cells were reseeded in T175 culture flasks.

3.2 Transfection with coding sequences for fluorescence proteins

Since the main part of the thesis incorporates the comparison between hypoxic and normoxic cultured myoblasts, a visual distinction of both was necessary. Therefore, the coding sequence (CDS) of the green fluorescent protein (GFP) and red fluorescent protein (RFP) were used to create new C2C12 cell lines. For the CDS insertion of the GFP and RFP, Amaxa Cell Line Nucleofactor Kit V, a sleeping beauty transposon system, was used.

The Sleeping Beauty (SB) transposon system is composed by a sleeping beauty transposase and a synthetic DNA transposon designed to insert precisely defined DNA sequences into genomes as a non-viral vector (92). The translocation works in a cut-and-paste manner. The SB transposase inserts the transposon into a recipient DNA sequence, i.e. in a duplicated TA dinucleotide base pair insertion site. (93, 94) (Fig.6).

For each fluorophore, 0.4 µl of the sleeping beauty transposon plasmide

(GFP: pSBbiGP, RFP: psBbiRP) (95) with 0.9 µg pCMV transposase (pCMV (CAT)T7-SB100) (96) and 20 µl nucleofactor solution (Amaxa Cell Line Nucleofactor Kit V, Lonza, Switzerland) were added to 500'000 cells. The cell/DNA suspension was transferred to the bottom of the certified cuvettes with cap and electroporated with a 4D-Nucleofector™ Core Unit (program B032, Lonza, Switzerland). After the nucleofection, 500 µl of GM were immediately added to the samples and they were gently transferred into a 6-well plate, with a final volume of 1.5 ml/well. The 6-well plate was incubated for 24 hours at 37°C in a 5% CO₂ and 95% humidified atmosphere, before 2 µg/ml Puromycin were added to the wells in order to eliminate cells without puromycin resistance.

After 10 days of puromycin selection, stably transfected cells were sorted by fluorescence-activated cell sorting (FACS) (FACS AriaFusion, BD, USA), in order to distinguish between high and low fluorescent protein expressing C2C12^{GFP} and C2C12^{RFP} cells. During FACS, a debris gate was applied to define the cells of interest.

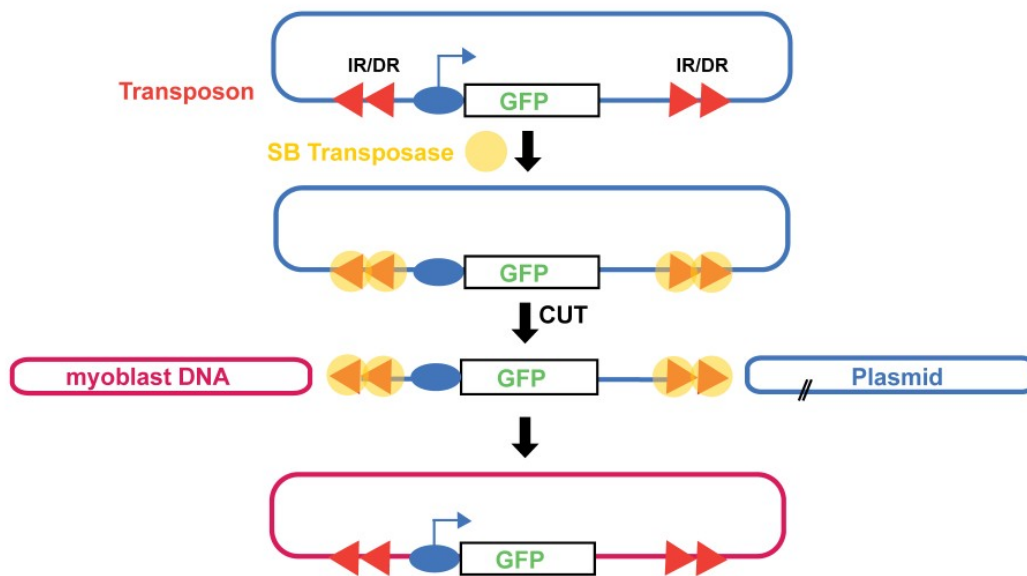


Figure 3.2: Transfection of fluorescent proteins into C2C12 cells by using a SB transposon system. The transposon consists of the genetic sequence of interest, in this case the coding sequence of GFP and RFP which is flanked by inverse repeats (IR) with short direct repeats (DR), allowing the SB transposase to locate the area of interest. By cut-and-paste mechanism, the sequence of interest is inserted into the DNA of C2C12 cells (myoblasts). However, a stable integration, can not be guaranteed.

Additionally, a singlets gate was applied to remove cell clumps that could interfere with the sorting process. After sorting, the cells were reseeded for another passage and afterwards, to maintain a certain cell pool for all further experiments, all sorted cells were frozen in nitrogen tanks. Therefore, trypsinization was performed as described above and the cells were counted. For each cryo vial, 1 million cells were resuspended in 70% GM, as well as with 10% dimethyl sulfoxide (DMSO) (Merck, Germany) and 20% FBS (Sigma Aldrich, USA). After the resuspension, the vials were immediately put into dry ice and stored in liquid nitrogen. For all further experiments described below, 1 million C2C12^{GFP} and just as many C2C12^{RFP} were seeded in T175 flasks. C2C12^{GFP} cells were incubated exclusively at 37°C in a 5% CO₂ and 95% humidified atmosphere, mimicking normoxia, and C2C12^{RFP} at 37°C in a 5% CO₂ / 2% O₂ incubator with a nitrogen inlet, mimicking hypoxia. For each series of experiment, new cells from the cell pool were thawed, in order to provide the same preconditions for all experiments. Only C2C12 mouse myoblasts up to passage 15 were used.

3.3 Morphological changes

The morphological changes due to oxygen levels < 2% O₂ over a period of 28 days were investigated. Respectively, each population was seeded in two T25 cell culture flasks, one incubated at 37°C in a 5% CO₂ and 95% humidified atmosphere and the other one at 37°C in a 5% CO₂ / 2% O₂ with a nitrogen inlet. Hence, it is possible to observe the impact of environmental changes within the myoblasts, regardless of their prior culturing circumstances.

Phase contrast images were acquired with an AxioObserver Z1 (Zeiss, Germany) of both culture groups (21% O₂ and 2% O₂) were taken once a week. Beginning at 24 hours after cell seeding, on day 9, 16 and finally day 23. In the end, to evaluate oxygen-related morphological changes of the cells over all passages, the image processing software ImageJ (NIH, USA) was used (97).

As not only the area is an important descriptor for cell morphology and therewith function, the aspect ratio (AR) was additionally measured. The latter one is a ratio describing the different dimensions within the myoblasts, including minimum and maximum diameters of the cells. To measure the area and the AR of the myoblasts at the different time points, the region of interest (ROI) manager was used and each cell was

marked manually, using the "freehand selection" tool. A total of 214 "normoxic" cultured cells and 252 hypoxic cultured cells were evaluated by this method.

3.4 Population doubling and population doubling time

Next, the cumulative population doubling (cumPD) and closely associated population doubling time (PDT) was investigated. The cumPD represents the total number of times, the cells in a given population have doubled during *in vitro* culture. It is commonly used for reporting cellular age *in vitro*. Regarding this case, it allows the direct comparison of the doubling of the myoblasts populations in two different oxygen saturations, without respect to their origin. The population doubling time refers to the duration required for a cell population to multiply in size or magnitude by two under a steady rate of growth. For this thesis, it was used to include the replication time of the myoblasts.

Similar to the prior experiment, duplicates of T25 cell culture flasks with either C2C12^{GFP} or C2C12^{RFP} were created and observed over a period of 28 days. Flasks were incubated either at 37°C in a 5% CO₂ and 95% humidified atmosphere or at 37°C in a 5% CO₂ / 2% O₂ incubator with a nitrogen inlet. Cell trypsinization and counting with the Neubauer counting chamber was carried out after 4, 7, 11, 14, 18, 21, 25 and 28 days. Only 50'000 of the counted cells were transferred into new cell culture flasks to continue the experiment. In the end, the cumPD was counted as following:

$$cumPD = \frac{\ln \frac{NE}{NB}}{\ln 2} \quad (3.1)$$

(NE is cell count at the end and NB the cell count in the beginning).

3.5 Myoblast fusion assay

To observe fusion among both cell populations, two six-well plates were seeded with 450'000 cells/well with either only C2C12^{GFP}, only C2C12^{RFP} or a mixture of both cell populations (C2C12^{GFP} + C2C12^{RFP}). One 6-well plate was incubated at 37°C in a 5% CO₂ and 95% humidified atmosphere and the other one at 37°C in a 5% CO₂ / 2% O₂

incubator with a nitrogen inlet. After 6 days some cells already started to differentiate and the GM was switched to differentiation medium (DM).

DM, containing DMEM with GlutaMAX I (Thermo Fisher, USA) supplemented with 2% horse serum (HS) (Sigma Aldrich, USA) was used. After day 2, a medium change took place. On day 4, within DM, newly formed myotubes were visualized by immunohistochemistry against myosin heavy chain 1E (MYH1E) (clone MF20, obtained from the Developmental Studies Hybridoma Bank developed under the auspices of the NICHD and maintained by The University of Iowa, Department of Biological Sciences, Iowa City, IA 52242).

Therefore, the cells were fixed for 15 minutes in PBS with 4% paraformaldehyde paraformaldehyde (PFA) (Merck KGaA, Darmstadt, Germany) and washed three times in PBS for 5 minutes at room temperature. The cells were blocked once for 1 hour in a blocking solution (0.5% Triton X 100 and 10% horse serum in PBS) at room temperature and incubated overnight at 4°C with the primary antibody, mouse anti MF20, (1:50 in blocking solution). Afterwards the cells were washed three times with PBS and incubated with fluorophore conjugated secondary donkey@mouse antibodies, Alexa 647, (1:500 in blocking solution, Thermo Fisher, USA) for 1 hour at room temperature. Afterwards, the cells were washed twice in PBS, counterstained with 4,6-Diamidine-2-phenylindole dihydrochloride (DAPI), in order to stain the nuclei. Then the cells were washed once more with PBS. In the end, the wells were mounted in Fluoroshield (Abcam, UK).

Subsequent, large overview images, covering slightly over 0.75 cm² (10 x 10 images per well), were acquired with the fluorescence microscope (AxioObserver, Zeiss Germany). Every image contains 4 channels, GFP-channel, RFP-channel, MYH1E-channel and DAPI-channel, which can be split or overlapped to highlight one or more feature(s).

3.6 Analysis of the relative number of myotubes

To quantify differences in myoblast fusion, the total number of MT was counted manually again by using the marking functionality in ImageJ. Thereby, three subgroups of the MT were distinguished, depending on their fused myoblasts. MT^{GFP} (C2C12^{GFP} fused with C2C12^{GFP}), MT^{RFP} (C2C12^{RFP} fused with C2C12^{RFP}) and MT^{GFP+RFP} (C2C12^{GFP}

fused with C2C12^{RFP}) (Fig. 3.3).

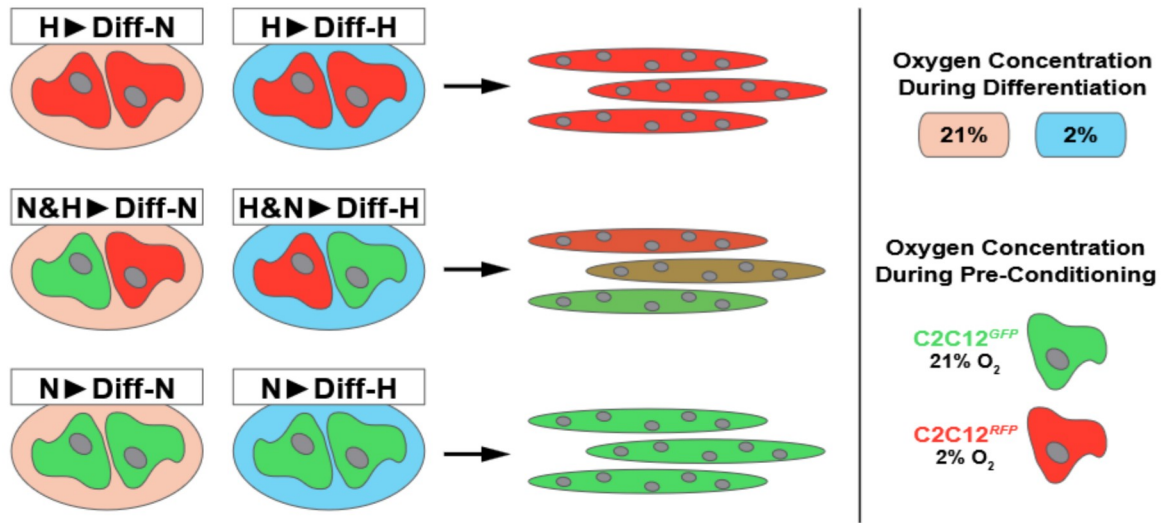


Figure 3.3: Experiment structure. C2C12^{GFP} cultured in 21% O₂ and C2C12^{RFP} cultured in 2% O₂ were mixed and further cultured in either hypoxic or normoxic environment to observe their interaction. After a confluence of > 50%, differentiation was induced by changing to DM. The visual distinction between the subgroups was due to their color. While, pure green myotubes indicated a fusion among C2C12^{GFP} (MT^{GFP}), pure red myotubes indicated to a fusion among C2C12^{RFP} cells only (MT^{RFP}). Myotubes consistent of both colors or showing an green/red color gradient, represented the fusion among C2C12^{GFP} and C2C12^{RFP} cells (MT^{GFP+RFP}), indicating an interaction between both populations. Adopted and modified from Pircher et al. (98).

To remove unfused myoblasts from the images, new composed images, only consisting of differentiated myotubes were created. Thereby, the GFP- and RFP-channel images were imported to ImageJ and converted to 8-bit (unsigned integer greyscale, [0-255]). A median filter of radius 2.0 pixels was applied to remove noise from the images and a manually determined threshold was applied. Afterwards, the MYH1E-channel image was imported, converted to 8-bit greyscale and merged through the image calculator with the above described newly created GFP- and RFP-channel. The resulting composite image therefore only includes pixels in MYH1E- and GFP- or MYH1E- and RFP-images. To finally recognize the different subgroups of the mixed myotubes (MT^{GFP}, MT^{RFP}, MT^{GFP+RFP}), both new composite images were merged by the channel merger of ImageJ. The cell count was performed manually using the ImageJ cell counter. To calculate the relative number of myotubes, the counted number of cells within the different subgroups, was related to the total number of myotubes within the image.

3.7 Analysis of the relative myotube area

Similarly to the experimental approach above, the total myotubes positive area within a well was determined by using ImageJ. In order to exclude empty areas, we determined a ROI, where we measured the total and fractional area of fused myoblasts.

To analyze the area within subgroups (MT^{GFP} , MT^{RFP} and $MT^{GFP+RFP}$), a self-made Python script (Python 3.7.6) was used and a sequence of standard automated image processing algorithms were applied. The libraries numpy (for matrix processing), scikit-image (for standard image processing algorithm implementations) and matplotlib (for visualization) were used. Three color channels, representing the RFP-channel (red), GFP-channel (green) and MYH1E-channel (blue) were loaded separately. These images show the cells within each of the channels (also inside the above defined ROI) in the corresponding color. In order to preserve the overall image pixel sum, a mono image is created by a mean over the three channels for each pixel:

$$I^{Mono}[x, y] = \frac{I^R[x, y] + I^G[x, y] + I^B[x, y]}{3} \quad (3.2)$$

With these single channel images the processing is done while being treated as greyscale frames. Similar to the method of defining the number of myotubes, the resulting images corresponding to the GFP-channel, RFP-channel and MYH1E-channel are converted to 8-bit. A median filter of 2 pixels and experimentally determined thresholds were applied. The values (listed in Table 3.1) were defined with the aim of getting fully closed cells while removing noise and outliers, experimentally.

The output of this thresholding operation is a binary image, showing cell associated pixels with a high value (i.e. 255) and non-related pixels with a low value (0). This boolean format helps proceeding with the upcoming logical operations. In order to determine, which cells are present within the "RFP-channel" and "MYH1E-channel" image and therefore, which correspond to fused $C2C12^{RFP}$, an overlap of the two images with a logical disjunction ($A \text{ AND } B$) is calculated, resulting in a new image C. The same procedure is applied with the "GFP-channel" and the "MYH1E-channel" image creating image C'. Further on, the "logical AND" operation is applied on the newly formed C and C' images to extract the myotubes consisting of both fluorescent proteins ($MF^{GFP+RFP}$), forming image D. In the end, image D is subtracted from image C and C' to get the area

	N&H►Diff-H	N&H►Diff-H	N&H►Diff-H	N&H►Diff-N	N&H►Diff-N	N&H►Diff-N
AK1	(19,28,9)	(24,25,20)	(24,25,11)	(25,19,24)	(27,20,15)	(23,19,17)
AK2	(12,7,10)	(19,21,10)	(18,20,10)	(21,16,11)	(25,12,12)	(23,10,20)
AK3	(20,22,16)	(16,27,14)	(24,31,12)	(21,18,19)	(19,18,15)	(19,13,18)
AK4	(10,23,9)	(14,18,8)	(21,28,10)	(26,26,7)	(14,16,7)	(17,18,9)

Table 3.1: Experimentally evaluated and applied thresholds for each image. Each line represents a series of experiments (n=4) called AK1-AK4. The line above refers to the environment and cell group, being evaluated (N&H►Diff-H or N&H►Diff-N). Each bracket vector corresponds to one well within a 6-well plate. The numbers within the vectors show the applied thresholds for the three channels: RFP-channel (position 1), GFP-channel (position 2) and MYH1E-channel (position 3).

for MF^{GFP} and MF^{RFP} , as otherwise, the overlap areas in C and C' would be respected twice in this calculation.

3.8 mRNA-isolation and sequencing

To identify potential candidate genes, involved in transcriptional changes, mRNA sequencing of eight sample groups was carried out. Therefore, duplicates of six-well plates were created like in the myoblast fusion assay experiments described above. Each duplicate was incubated at either 37°C in a 5% CO₂ and 95% humidified atmosphere or at 37°C in a 5% CO₂ / 2% O₂ incubator with a nitrogen inlet and cultured for 24, 72, 96 or 144 hours.

Afterwards, RNA was isolated with Direct-zol™ by disposing the cell medium of the wells, quickly wash them with PBS and finally after PBS disposure, initiating cell lysis by applying 1 ml Trizol (Invitrogen, USA) per well. With a cell scraper (Sarstedt, Nümbrecht, Germany), the lysed cell material and the isolated RNA was detached and RNA integrity was validated with a Bioanalyzer (Agilent, USA) following a standard protocol. Afterwards, the isolated RNA was transferred to low DNA/RNA binding Eppendorf tubes and frozen at -20°C until RNA libraries preparation. Since myoblasts quickly adjust to a higher oxygen level, the RNA isolation needed to be done quickly, in order to make sure, that no oxygen induced changes within the cells were reversed. To generate the RNA-sequencing libraries, the SENSE mRNA-Seq Library Prep Kit V2 (Lexogen, Vienna, Austria) according to the manufacturers' protocol was used and sequencing was

performed on a HiSeq1500 device (Illumina, San Diego, CA, USA) with a read length of 50 bp and a sequencing depth of approximately 6 million reads per sample. In the end, a total of 48 isolated RNA samples were sequenced by the Gene Centre of the Ludwig-Maximilians-University Munich.

3.9 Bioinformatic analyses

FASTQ files were demultiplexed by the sample specific barcodes used for generation of each library. Reads were aligned to the mus musculus genome (release GRCh38.99) using STAR (version 2.7.2b). Afterwards, gene counts less than 10 reads per gene over all samples were filtered out. For further analyses 22,105 genes were remaining, which were normalized through variance stabilizing transformation (VST) for Principal Component Analysis (PCA). Differential gene expression was analyzed by DESeq2 package (version 1.28.1) in R software (version 4.0.3) with adjusted p-value (p-adj) of 0.05 and a Log2FoldChange of ± 2 cut off for each condition and each time point.

Additionally, a Venn diagram was created, including significantly differently expressed genes over all four time points with a p-adj value of < 0.05 . In the end, a gene set enrichment analysis (GSEA) in each time point was performed using org.Mm.eg.db (version 3.11.4) and mouse_H_v5 hallmark gene set from the Molecular Signatures Database (MSigDB) R package (version 7.0).

3.10 Statistical analysis

Except for the myoblast fusion assay experiment, which was carried out four times, all experiments were repeated at least three times in duplicates. Statistical significance was calculated after determination of a Gaussian distribution using either a one-way ANOVA test or a T-test with appropriate post hoc tests in R (version 4.1.0). At a p-value of ≥ 0.05 , statistical significance was assumed. Data is represented as either the mean and standard deviation (SD) or the median with quartiles.

Chapter 4

Results

4.1 Prolonged hypoxic exposure affects the morphology of C2C12 myoblasts but does not change their proliferation

Starting with the long-term effects of hypoxia onto myoblast cell morphology, C2C12 were exposed to 2% O₂ over a period of 4 weeks. Afterwards, visible differences between 21% O₂ (Fig. 4.1 [A]) and 2% O₂ (Fig. 4.1 [B]) were observed microscopically. At direct comparison of the measured area and aspect ratio within both groups, slight morphological changes during prolonged hypoxia were observed (Fig. 4.1 [A',B']). A quantification of the cell area showed no significant morphological changes in hypoxia, when compared to the normoxic control group (Fig. 4.1 [C]). However, analyzation of the aspect ratio revealed a slightly rounder cell phenotype in the hypoxic group in comparison to cells in normoxia. The aspect ratio of the C2C12 cells within 2% O₂ was 16% lower ($AR = 2.389 \pm 1.111$), when compared to cells in 21% O₂ ($AR = 2.771 \pm 1.342$), indicating less elongation and more width (Fig. 4.1 [D]).

Apart from morphological changes, the long-term hypoxic effects on the proliferation were investigated. Therefore, quantifications of cumulative population doubling and duplication time were performed over 28 days. Up to day 7, the cumPD at 2% and 21% O₂ were very similar. At day 28, a 6.2% lower cumPD within the hypoxic group (cumPD 43.065 ± 2.620) was observed, compared to normoxic cells (cumPD 45.725 ± 1.359) (Fig. 4.1 [E]). Subsidiary, the population doubling time was measured, which did

not show significant differences between both oxygen levels, indicating no long-term hypoxia effect onto proliferation. After 28 days the PDT for 21% O₂ resulted in PDT 0.618 ± 0.102 days and for 2% O₂ in PDT 0.663 ± 0.127 days (Fig. 4.1 [F]).

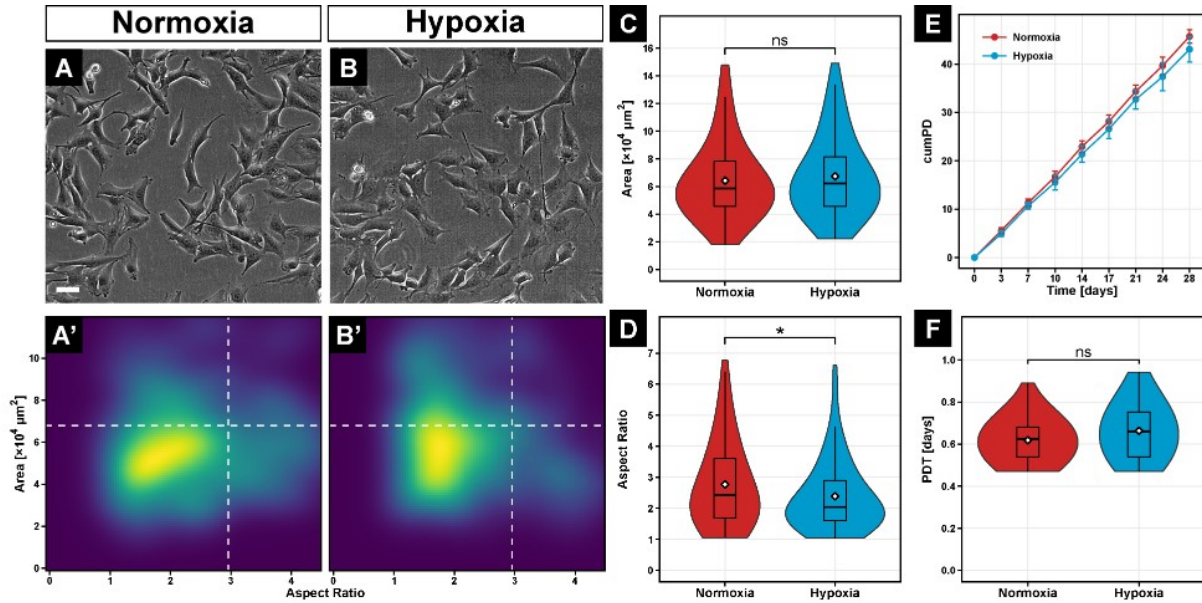


Figure 4.1: Morphology and proliferation in hypoxia. Phase-contrast images of C2C12 cells exposed to 21% O₂ (A) compared 2% O₂ (B) showed visible differences, which were also shown by direct comparison of the cell area and AR (A'/B'). Quantification of the individual cell morphology parameters revealed a significant decrease of the aspect ratio (D), but not of the area (C) within 2% O₂. The effects of hypoxia on proliferation were evaluated with the cumulative population doubling (E) and the population doubling time (F) over a period of 28 days, showing no significant differences between normoxia and hypoxia. Violine plots represent the median and quartiles. *equals $p \leq 0.05$, ns.: not significant. Adopted and modified from Pircher et al. (98).

4.2 *In vitro* myoblast fusion is inhibited by long-term hypoxia

The next observation shows the effect of long-term 2% hypoxia on myogenic differentiation. To identify newly formed myotubes, an immunostaining against MYH1E (myosin heavy chain) was performed. After 7 days, C2C12 cells showed less myotube formation in 2% O₂ compared to 21% O₂ (Fig. 4.2 [A]). The relative myotube area was 70.62% smaller (Fig. 4.2 [B]) within 2% O₂ (29.360 ± 3.777), when compared to 21%

O₂ (100.002 ± 19.102) The relative number of myotubes was 55.98% lower in hypoxia (43.410 ± 8.842) in comparison to C2C12 cells in normoxia (98.604 ± 22.129) (Fig. 4.2 [C]).

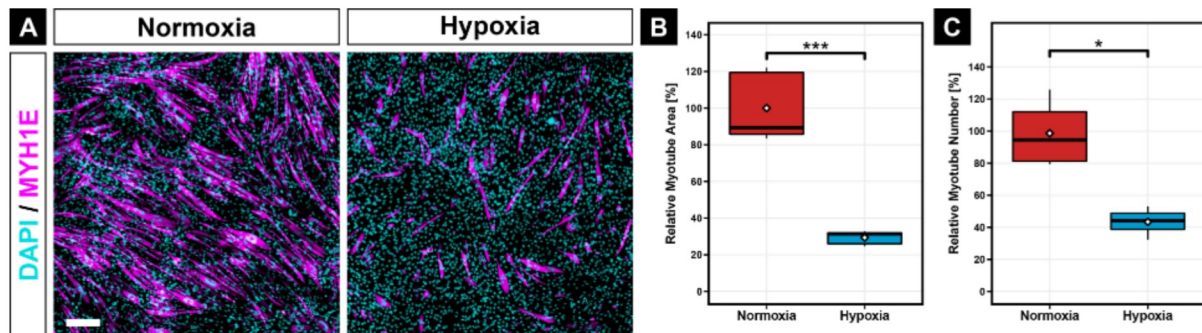


Figure 4.2: Myoblast fusion during hypoxia. MYH1E-immunohistochemistry (magenta) after 7 days of myogenic differentiation, showed higher count of newly formed myotubes in 21% O₂, compared to 2% O₂ (A). Quantification of relative myotube area (B), as well as relative myotube number (C) revealed significantly reduction of myoblast fusion in an oxygen concentration of 2%. Scale bar: 200 μ m. Box plots represent the median, quartiles, range and mean (white diamond). Significance levels: *equals $p \leq 0.05$; ***equals $p \leq 0.001$. Adopted and modified from Pircher et al. (98).

4.3 Novel myoblast fusion assay used to analyze interaction of normoxic and hypoxic conditioned myoblasts

Depending on the extent of damage in skeletal muscle cells after injuries, myoblasts are exposed to an initial hypoxic environment, until proper blood flow is restored. This thesis assumed an interaction of different oxygen-conditioned myoblasts and therefore investigated the fusion of normoxic and hypoxic-conditioned myoblasts. C2C12 cell lines stably expressing a green (GFP; used for normoxic C2C12 myoblasts) or red (RFP; used for hypoxic C2C12 myoblasts) fluorescence protein, were generated as described above. Thereby, the C2C12^{GFP} cells were exclusively cultured in 21% O₂ and the C2C12^{RFP} cells in 2% O₂, before using them for the differentiation assay.

During transfection, a loss of myogenic differentiation capacity is possible, since the insertion of a fluorophore coding sequence along the DNA is not controllable. To exclude possible transfection-induced change of myogenic differentiation potential be-

fore addressing the main research question of this thesis, the fusion experiment was repeated with the newly created cell lines (C2C12^{GFP} in 21% O₂, C2C12^{RFP} in 2% O₂).

No significant changes of myoblast fusion within immunohistochemistry were observed, when compared to non-transfected C2C12 cells (Fig. 4.3 [A-B]). The fusion of transfected myoblasts showed an obvious accumulation of fluorescence intensity. (Fig. 4.3 [A-B'], arrowheads).

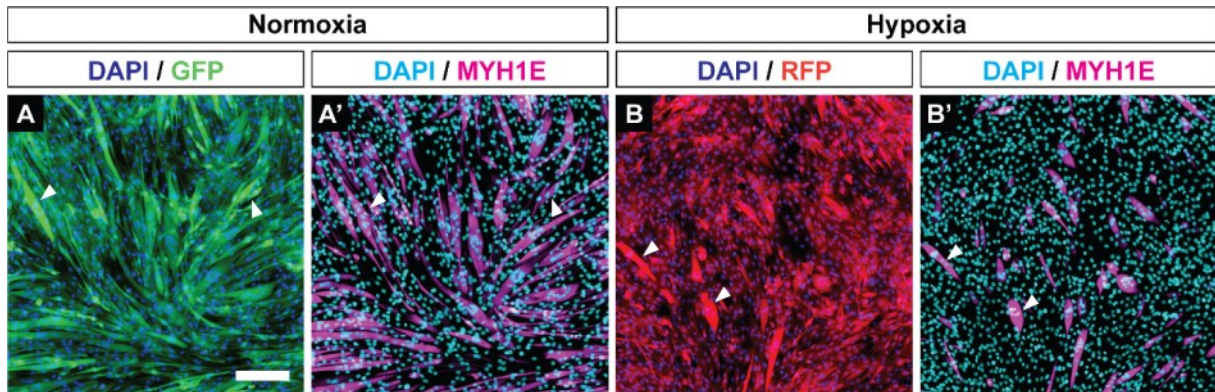


Figure 4.3: Differentiation after transfection of GFP and RFP coding sequence into C2C12 cells. Formed myotubes with their nuclei are shown by staining with DAPI and immunohistochemistry against MYH1E. The arrows indicated the myotubes, showing no impact on myoblast fusion by the insertion of the fluorescent proteins in neither normoxia (A') nor hypoxia (B'). Scale bar: 200 μ m. Adopted and modified from Pircher et al. (98).

4.4 Myogenic differentiation of normoxic and hypoxic preconditioned myoblasts is affected by abrupt changes of oxygen concentrations

In all further experiments a unified labelling of the experimental group is used. Hence, 21% O₂ is labeled with 'N' (normoxia) and 2% O₂ with 'H' (hypoxia). The overall label consists of two parts. The first one before the arrow, denotes normoxic or hypoxic-conditioning of the used C2C12 myoblasts, while the part after the arrow reflects the oxygen treatment during subsequent differentiation. For example, 'N&H►Diff-H' refers to a mix of normoxic ('N') and hypoxia ('H') conditioned myoblasts that are subsequently differentiated in 2% O₂.

Prior to the mixed cell line differentiation assays, the impact of abrupt changes of oxygen concentration onto myogenic differentiation was analyzed. Therefore, long-term hypoxia-conditioned C2C12^{RFP} myoblasts were differentiated in normoxia (H►Diff-N) and normoxia-conditioned C2C12^{GFP} myoblasts in 2% O₂ (N►Diff-H). A direct comparison between H►Diff-N (Fig. 4.4 [A,A']) and N►Diff-H (Fig. 4.4 [C,C']) myotubes did not show significant differences in the overall myogenic efficiency (Fig. 4.4 [E]), the number (Fig. 4.4 [F]) or size of the myotubes (Fig. 4.4 [G]). Nevertheless, when comparing differentiation of hypoxic conditioned cells in the two different oxygen concentrations, 5% increased efficiency in myogenic differentiation, as well as a 19% higher number of myotubes and 13% larger myotube size was observed within H►Diff-N, when compared to H►Diff-H (Fig. 4.5). For the normoxic cell line, 67% lower total myotube area and 48% fewer number of myotubes were observed within N►Diff-H, when compared to N►Diff-N. Moreover, the myotubes within N►Diff-H showed 33% smaller size compared to N►Diff-N (Fig. 4.5).

Those findings suggest that the negative effect of hypoxia on myogenic differentiation is partially reversible. Besides, hypoxia leads to a decreased number, but significantly larger sizes of myotubes and is therefore suggested to be partially involved in myotube hypertrophy.

4.5 Fusion of hypoxic with normoxic conditioned myoblasts results in larger myotubes

Next, the effect on the myogenic differentiation of the mixture of hypoxic- and normoxic conditioned myoblasts under either normoxia or hypoxia was investigated. During the following differentiation assay, all interactions between the two cell lines were expected to be detected by the color of the newly formed myotubes, indicating the extent to which C2C12^{GFP} and C2C12^{RFP} myoblasts fused. It was differentiated between red (C2C12^{RFP}), green (C2C12^{GFP}) and yellow myotubes (C2C12^{GFP} and C2C12^{RFP}).

Since prior studies showed a positive impact of hypoxic preconditioning on myoblast differentiation (36), this thesis expected to see similar results for our mixed cell line, differentiated within 21% O₂ (N&H►Diff-N). Indeed, more myotube formation was microscopically detected within differentiation at 21% O₂ (N&H►Diff-N ; Fig. 4.4 [B,B']),

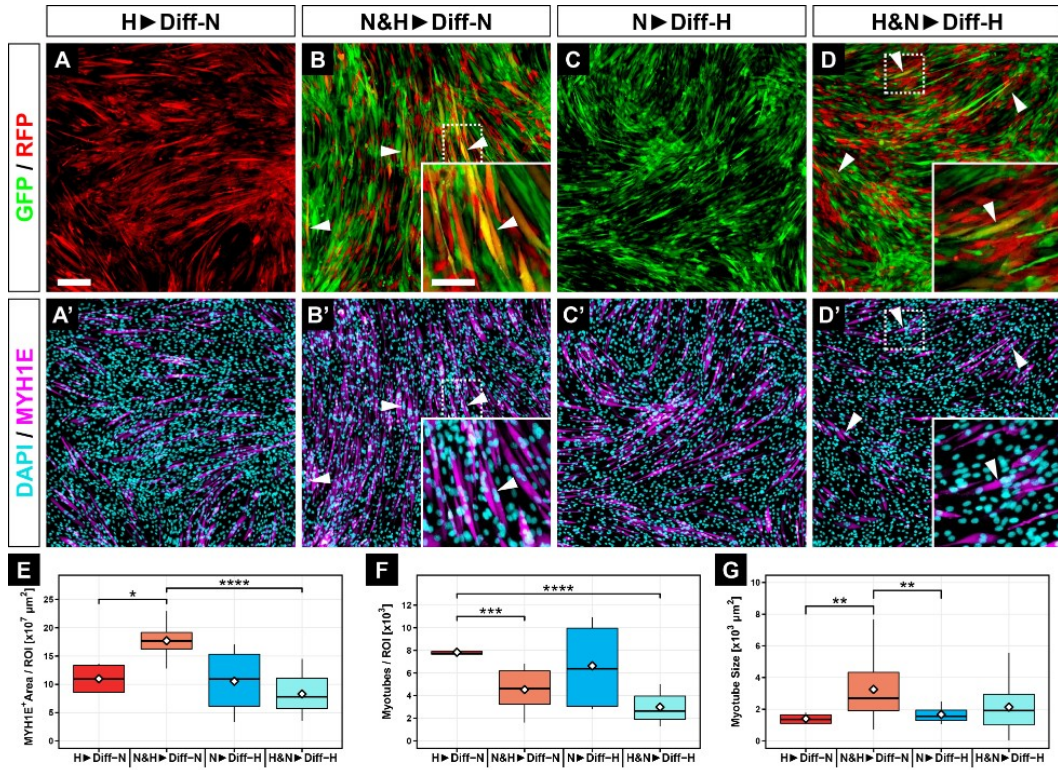


Figure 4.4: Fusion of hypoxic with normoxic conditioned myoblasts. Fluorescence microscope images (A-D) and the immunohistochemistry against MYH1E and DAPI (A'-D'). C2C12^{RFP}, differentiated within 21% O₂ (N&H>Diff-N, A/A') and the mixed culture within 2% O₂ (N&H>Diff-H, D/D') showed less myoblast fusion, when compared to C2C12^{GFP} differentiated in hypoxia (N>Diff-H, C/C') or the mixed group in normoxia (N&H>Diff-N, B/B'). Within the mixed cultured group, myotube formation by fusion of C2C12^{GFP} and C2C12^{RFP} was observed (B/D arrowheads). The greatest MF20⁺ area (myotube area, E) and the greatest myotube size (G) was observed within N&H>Diff-N. However, the mixing of C2C12^{GFP} and C2C12^{RFP} did not affect the number of myotubes (F) independent of their differentiating condition, compared to H>Diff-N. Scale bars: 200μM. Bar plots represent the median, quartiles, range and the mean (white diamond). *equals $p \leq 0.05$. **equals $p \leq 0.01$. ***equals $p \leq 0.001$. ****equals $p \leq 0.0001$. Adopted from Pircher et al. (98).

compared to 2% O₂ (N&H>Diff-H ; Fig. 4.4 [D,D']). Moreover, mixed myoblasts differentiated in normoxia formed 53% larger myotubes (MF20⁺ area N&H>Diff-N: $1,7 \times 10^7 \pm 2,9 \cdot 10^6 \mu\text{m}^2$), than during hypoxic differentiation (MF20⁺ area H&N>Diff-H: $8,2 \cdot 10^6 \pm 3,6 \cdot 10^6 \mu\text{m}^2$) (Fig. 4.4 [E]). However, compared to H>Diff-N (7831.500 ± 270.947), both mixed cultured showed a lower number of myotube formation. A 42.13% reduction within N&H>Diff-N (4531.917 ± 1789.771) and a 61.86% reduced myotube formation in H&N>Diff-H (2987.250 ± 1298.791) was observed (Fig. 4.4 [F]). Additionally, the single myotube size was evaluated. Thereby, a greater myotube size in N&H>Diff-N ($4752.569 \pm 2727.073 \mu\text{m}^2$), compared to N>Diff-H (1665.210 ± 615.763

μm^2) or H►Diff-N ($1400.153 \pm 347.811 \mu\text{m}^2$) was observed (Fig. 4.4 [G]).

To summarize the previous findings, all investigated groups were normalized to N►Diff-N. Thereby, several additional observations were made. The mixture of hypoxic with normoxic cells reduce myotube formation within normoxia (N&H►Diff-N), resulting in 42% reduced MYHE⁺ area and 64% decreased number of myotubes, when compared with N►Diff-N (Fig. 4.5). 14% larger myotubes were formed when differentiated under hypoxia (N&H►Diff-H), compared to N►Diff-N. Comparison of the mixed and single cell population groups, the lowest number of myotubes was observed within both mixed groups, independent of their environment of differentiation (N&H►Diff-H and N&H►Diff-N) (Fig. 4.5).

Of particular note, the biggest relative myotube size among all compared groups was observed within N&H►Diff-N. A 91% higher myotube size in N&H►Diff-N was observed, compared to N►Diff-N (Fig. 4.5).

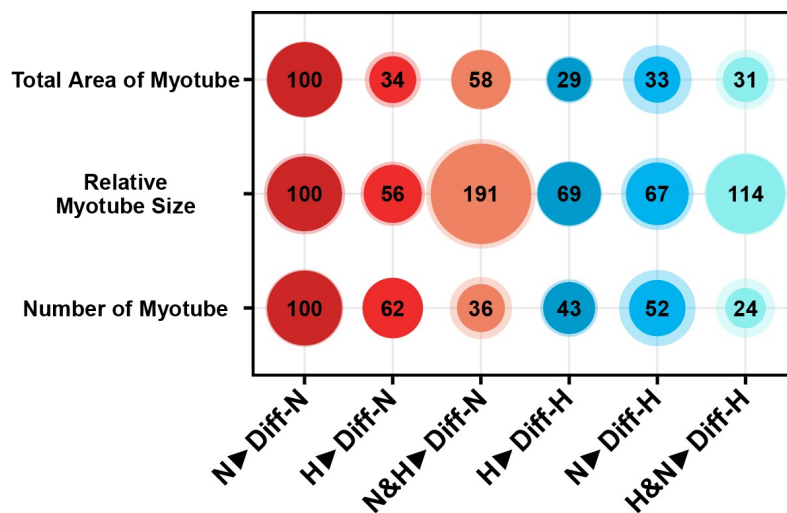


Figure 4.5: Bubble plot of all investigated groups, normalized to N►Diff-N. Within both mixed groups, the total number of myotubes was the lowest and revealed the largest relative myotube size. Especially within N&H►Diff-N the relative myotube size was greater, when compared to all other groups. Adopted and modified from Pircher et al. (98).

4.6 Oxygen Tension Differentially Influences Cell Fusion among Different Precultured Cell Populations

For a better understanding of the interaction between normoxia- and hypoxia-conditioned myoblasts during the fusion process in the mixed myotubes, the newly formed myotubes were divided into three subgroups, depending on which myoblasts were involved in the fusion process: MT^{GFP} , MT^{RFP} and $MT^{GFP+RFP}$. Quantification of area, number and size of the myotubes were performed as prior, including the absolute (Fig. 4.6 D-F) and relative values (Fig. 4.6 [A-C]) within an experimental group, as the oxygen concentration might influence the fusion properties of the subpopulations.

While the relative area of myotubes did not reveal any differences between 21% (N&H►Diff-N) and 2% (N&H►Diff-H) O_2 among all subpopulations (Fig. 4.6 [A]), the absolute values showed significant increases of all three groups within normoxia. The largest difference was noticed with a 316% increase of the absolute area within $MT^{GFP+RFP}$, while the least difference with 128% was observed at MT^{GFP} (Fig. 4.6 [D]).

A significant relative increase of the number of myotubes in $MT^{GFP+RFP}$ and a relative decrease of the number of myotubes in MT^{GFP} and MT^{RFP} within hypoxia was observed, compared with the groups oxygenated in 21% (Fig. 4.6 [B]). This effect was not noticed within the absolute number of myotubes. No significant changes within the double-fluorescent myotubes were observed. However, still significantly lower MT^{GFP} and MT^{RFP} formation was noticed within hypoxia (Fig. 4.6 [E]).

As for the relative and absolute myotube size, approximately 70% smaller $MT^{GFP+RFP}$ were detected within hypoxic differentiation (N&H►Diff-H)(Fig. 4.6 [C,F]).

4.7 Hypoxia Leads to Delayed Expression of Genes Encoding Regulators of Myogenic Differentiation

RNA-sequencing was performed to analyze the effect of oxygen on the transcriptional adaptation of myoblasts during differentiation within 21% (N&H►Diff-N) and 2% (N&H►Diff-H). After the onset of differentiation, the RNA-sequencing was performed at 4 different time points: 24, 72, 96 and 144 hours. Potential clustering was visualized

Results

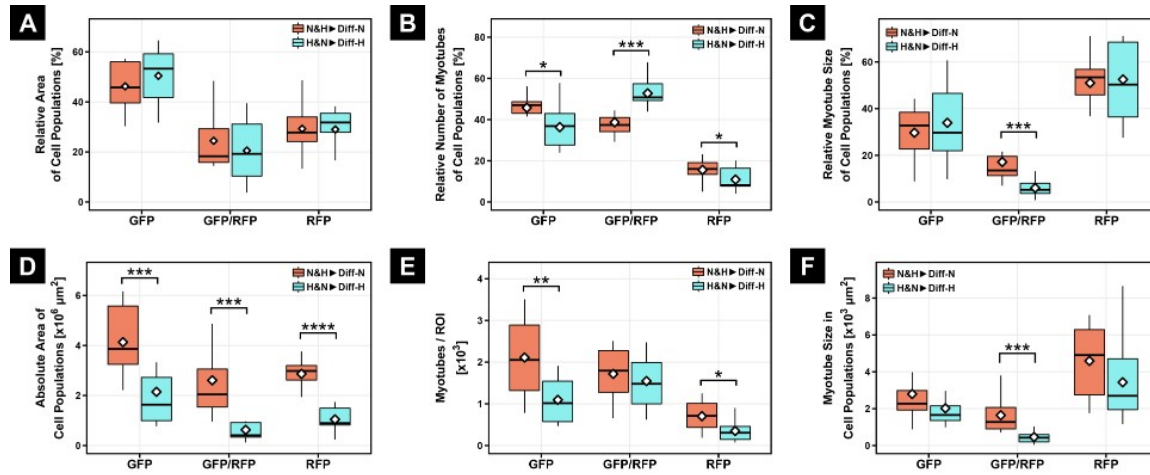


Figure 4.6: Analyses of the area, number and size of myotube subpopulations. Therefore, the relative and the absolute values were used. While no substantial differences were observed within the relative area of the subpopulation (A), a significant increase within the absolute values for the area of all subpopulations was noticed in 21% O₂ independent of the subpopulation (D). The relative number of myotubes showed a significant increase in double-fluorescent myotubes in hypoxic conditions, whereas within normoxia, the single-fluorescent myotubes with GFP predominate (B). However, the absolute number of myotubes did not show similar results (E). Regardless of their relative or absolute number, the myotubes size was significantly larger within all subgroups at 21% O₂, when compared to 2% O₂ (C & F). Bar plots represent the median, quartiles, range and mean (white diamond). *equals $p \leq 0.05$, **equals $p \leq 0.01$, ***equals $p \leq 0.001$, ****equals $p \leq 0.0001$. Adopted and modified from Pircher et al. (98).

by performing a PCA. Thereby, the main focus was on PC1, the time dependent first principal component (Fig. 4.7 [A], colored spheres), and PC2, the oxygen-dependent second component (Fig. 4.7 [A], shapes), which showed clear separation. A slight overall transcriptional delay of the hypoxic differentiated group (H&N►Diff-H, Fig. 4.7 [A], dots), when compared to N&H►Diff-N (Fig. 4.7 [A], triangles) was observed. Noteworthy, the mixed cells after 144 hours within hypoxia (Fig. 4.7 [A], violet dots) showed a proximity to the mixed C2C12 cells in normoxia after 72 hours (Fig. 4.7 [A], green triangle).

Differential gene expression (DEG) analysis revealed that 177 out of 6740 genes shown in the venn diagram, show an overlapping expression within all four different time points (Fig. 4.7 [B]).

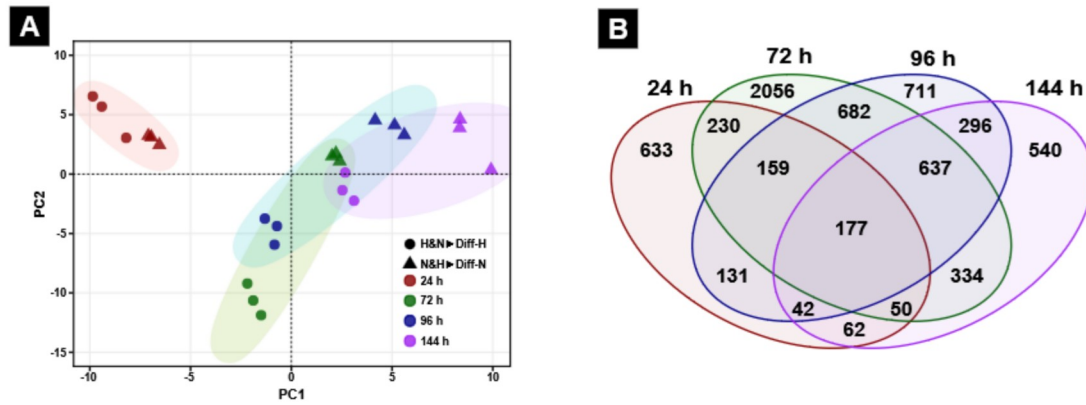


Figure 4.7: PCA and venn diagram. The PCA reveals a clear separation of H&N>Diff-H and N&H>Diff-N after 72 hours along the main component (PC1). Also, along PC2 a distinction of both groups is visible. A slight overall transcriptional delay of the hypoxic differentiated group (dots), when compared with to normoxia (triangles) was observed (A). The venn diagram shows for every time point the most significant changed genes and their overlapping expression between the different time points (B). Adopted and modified from Pircher et al. (98).

In addition, for a better understanding of the different pathway regulation within N&H>Diff-N and N&H>Diff-H, a gene set enrichment analysis (GSEA) was performed at all four time points. Thereby especially the hallmarks for 'hypoxia', 'glycolysis' and 'myogenesis' (Fig. 4.8 [A]) were observed. The significantly increase of 'myogenic' hallmark at 72 and 96 hours after initiation of differentiation, highlights the adaptive phase for H&N>Diff-H, when compared to N&H>Diff-N (Fig. 4.8 [A], lower panel).

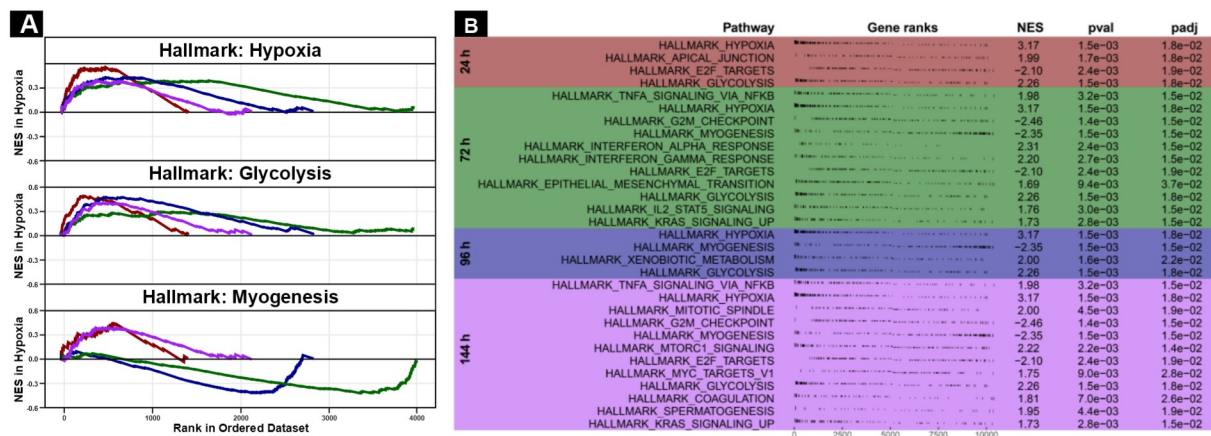


Figure 4.8: Visualization of the hypoxia dependent hallmarks over the four time points. Most positively (normalized enrichment score (NES) > 0) or negatively (NES < 0) hypoxia-dependent hallmark gene sets in myoblast group N&H>Diff-H, when compared to normoxic group, N&H>Diff-N, at the four different time points (A). All significant regulated gene set hallmarks detected (B). Adjusted p-value < 0.05 (C). Adopted and modified from Pircher et al. (98).

All significant regulated gene set hallmarks per time point are included in Fig 4.8 B. Within the first 72h, the relevant expressed hallmarks are predominantly related to inflammation, including interferon alpha (IFA) and interferon gamma (IFG) response, interleukin 2-signal transducer and activator of transcription 5 (IL2-STAT5) and tumor necrosis factor alpha (TNFA) signalling (4.8, green panel). After 144 hours, mainly myogenesis and hypoxia-related hallmarks, including mammalian target of rapamycin complex 1 (MTORC1) and Kirsten Rat Sarcoma gene (KRAS) signalling, E2F targets and myogenesis were present (Fig. 4.8 [B], violet panel).

In addition to the hallmarks, the following heat maps show top 50 genes contributing the most to PC1 or PC2. Thereby, it is remarkable, that PC1 contributing genes (Fig. 4.9 A), are myogenic-related marker genes, as for example *Myf4*, *Myh3*, *Tnni2*, *Tnnt3*, *Myh3*, *Casq2*, *Mymx*, *Mylpf*, *Mybph* and *Tnnc1*. Whereas, the genes in PC2 are associated with the adaption of myoblasts during hypoxia (Fig. 4.9 B), including *Car9*, *Efemp1*, *Sfrp4*, *Adm*, *Nos2*, *Aire*, *Apln*, *Gpr35*, *X2610528A11Rik*, *Ptgfr* and *Scara5*.

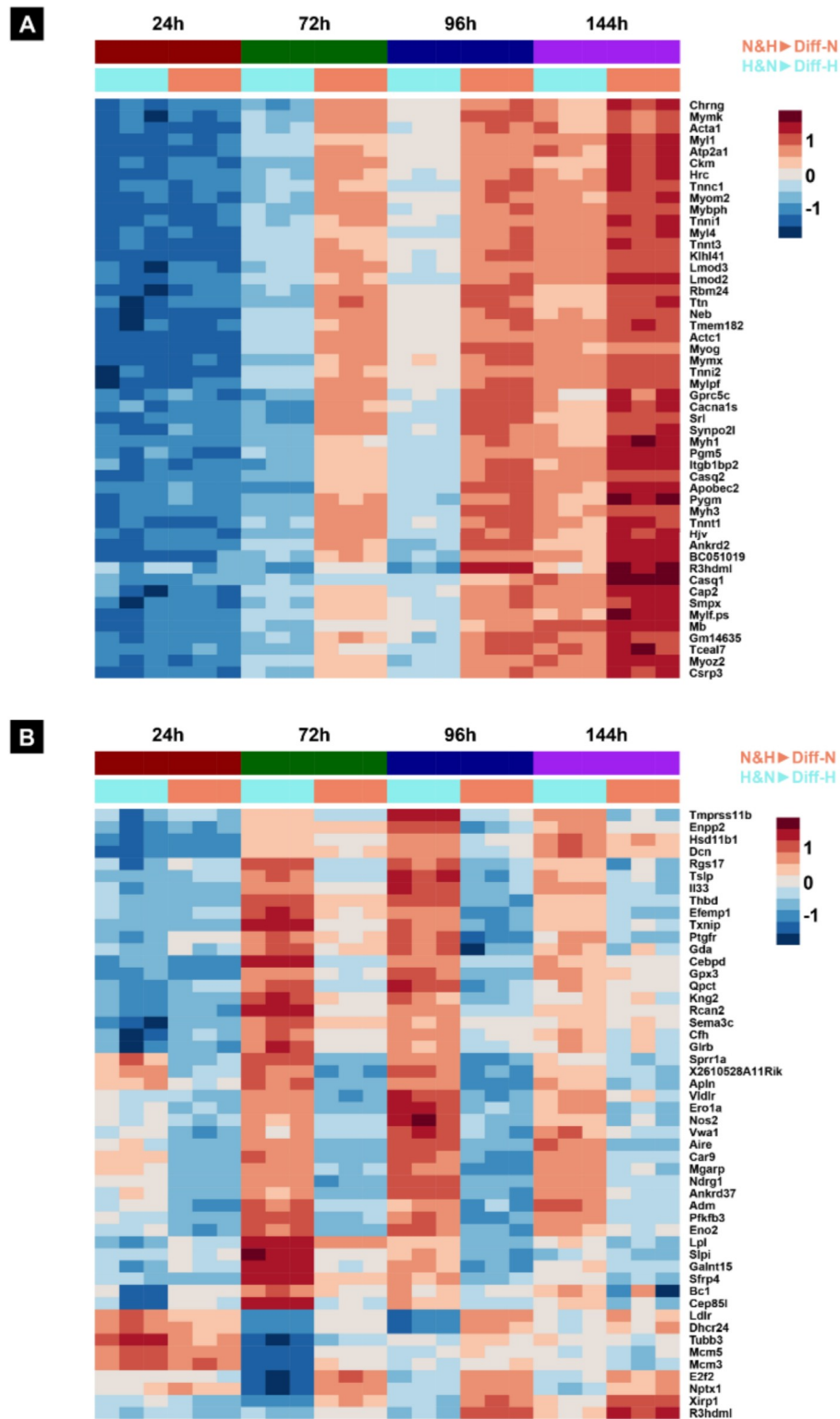


Figure 4.9: Heatmap of the top 50 to PC1 (A) or PC2 (B) contributing genes. All genes are sorted by their impact, listing the genes with the highest to each PC contributing on top of the map and those with the least contributing at the bottom.

For each measured time point between 24 and 144 hours a volcano plot was generated, including both cell groups (N&H►Diff-N and H&N►Diff-H) and highlighting the 20 most differentially regulated genes. Thereby, a negative log2foldchange (LFC) refers to a higher expression within N&H►Diff-N, while a positive log2foldchange refers to a higher expression within H&N►Diff-H.

After 24 hours, genes with a negative LFC include *Scara5*, encoding a ferritin receptor necessary for cell growth (99) and *Kcna4*, encoding for a voltage-gated potassium channel (100). Genes with a positive LFC include *Carboxy anhydrase 9 (Car9)* one of the most highly expressed genes in the hypoxic environment of solid tumors (101); *G-protein related receptor 35 (Gpr35)* encoding G-protein involved in ERK1/2 activation (102); *autoimmune regulator gene (Aire)* (103); *Adm*, encoding angiogenetic factor (104) and *X2610528A11Rik* (Fig. 4.10).

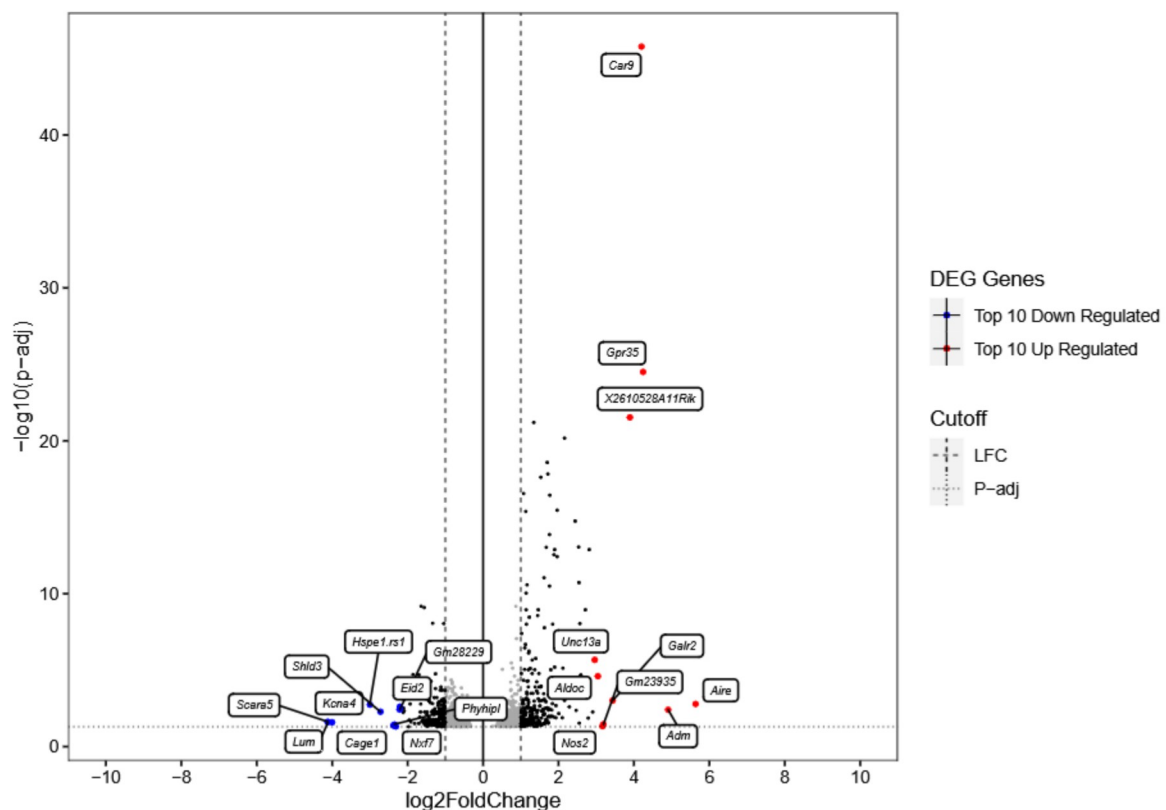


Figure 4.10: Volcano plot of the most differentially regulated genes 24 hours after start of myogenic differentiation. The plot reveals all higher regulated genes. Thereby, the TOP 10 genes for the positive and negative log2foldchange were visualized by color and naming. P-adjust < 0.05.

Not shown in the volcano plot, but also upregulated from 24h upwards was the CDH2 (Table S1 from Pircher et al. (98)), a hypoxia-sensitive cathepin, probably involved in myogenesis.

After 72 hours *Car9*, *X2610528A11Rik*, *Gpr35*, *Adm*, *Aire* are still higher expressed within N&H►Diff-H, followed by *Apelin* (*Apln*), known for the regulation of cell proliferation in smooth muscle cells (105); and *Spr2g*. However, the genes with a negative LFC change completely. *Slc44a4*, encoding for thiamine pyrophosphate transporter (106); *Slc2a6*; *Ms4a8a*; *Exo1*, encoding for 5' to 3' exonuclease (107); and *Gm13398* presented with a negative LFC after 72 hours (Fig 4.11).

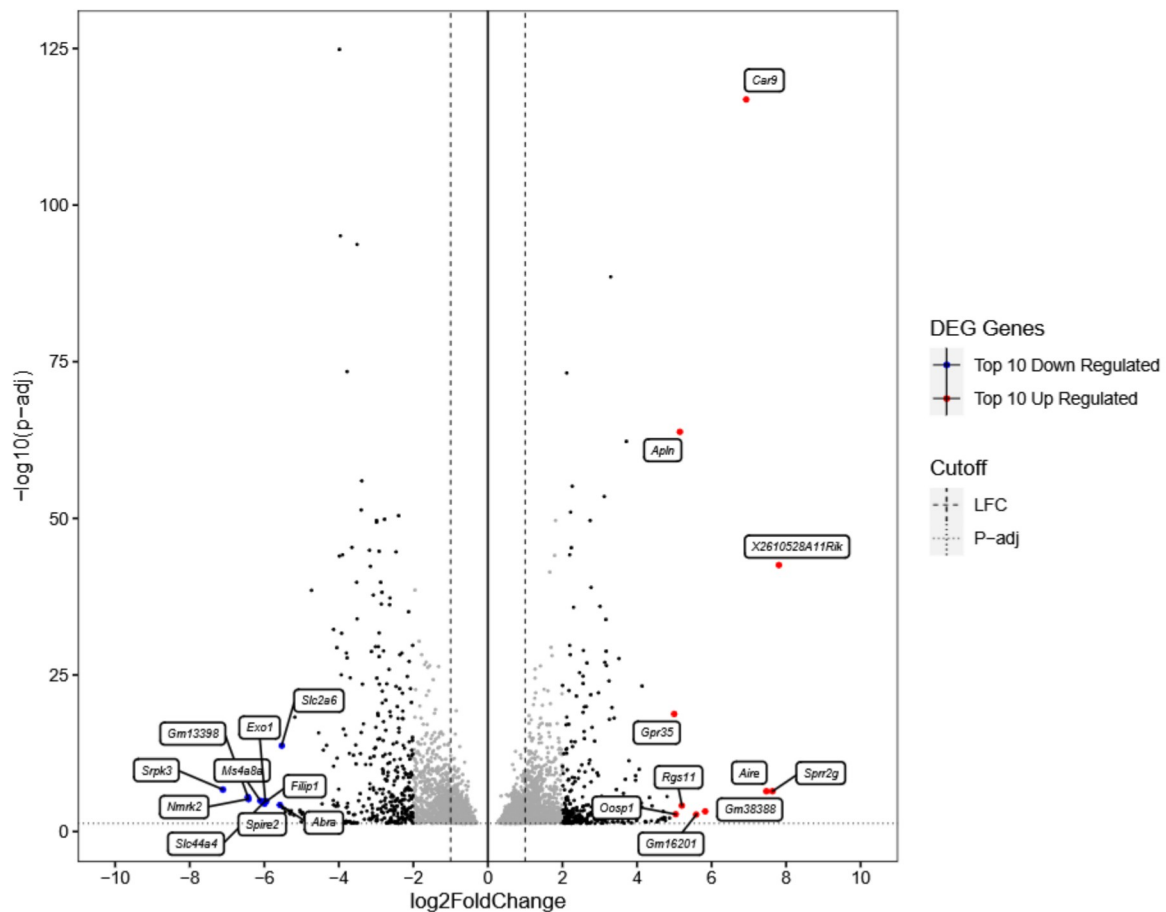


Figure 4.11: Volcano plot of the most affected genes after 72 hours. The plot reveals all higher regulated genes. Thereby, the TOP 10 gens for the positive and negative log2foldchange were visualized by color and naming. P-adjust < 0.05.

While *Car9*, *Apln*, *X2610528A11Rik* and *Aire* are still upregulated after 96 hours within H&N►Diff-H, the former downregulated *Kcna4*, *nitric oxide synthase 2 (Nos2)*, encoding NO synthase (108); and *Serpina3n*, encoding for serine protease inhibitor (109) are upregulated, afterwards. Similar to 72 hours, higher expressed genes within N&H►Diff-N changed significantly compared to prior time points. Noticeable is the up-regulation of *R3hdml*, known for its presence during satellite cell differentiation (110) (Fig. 4.12).

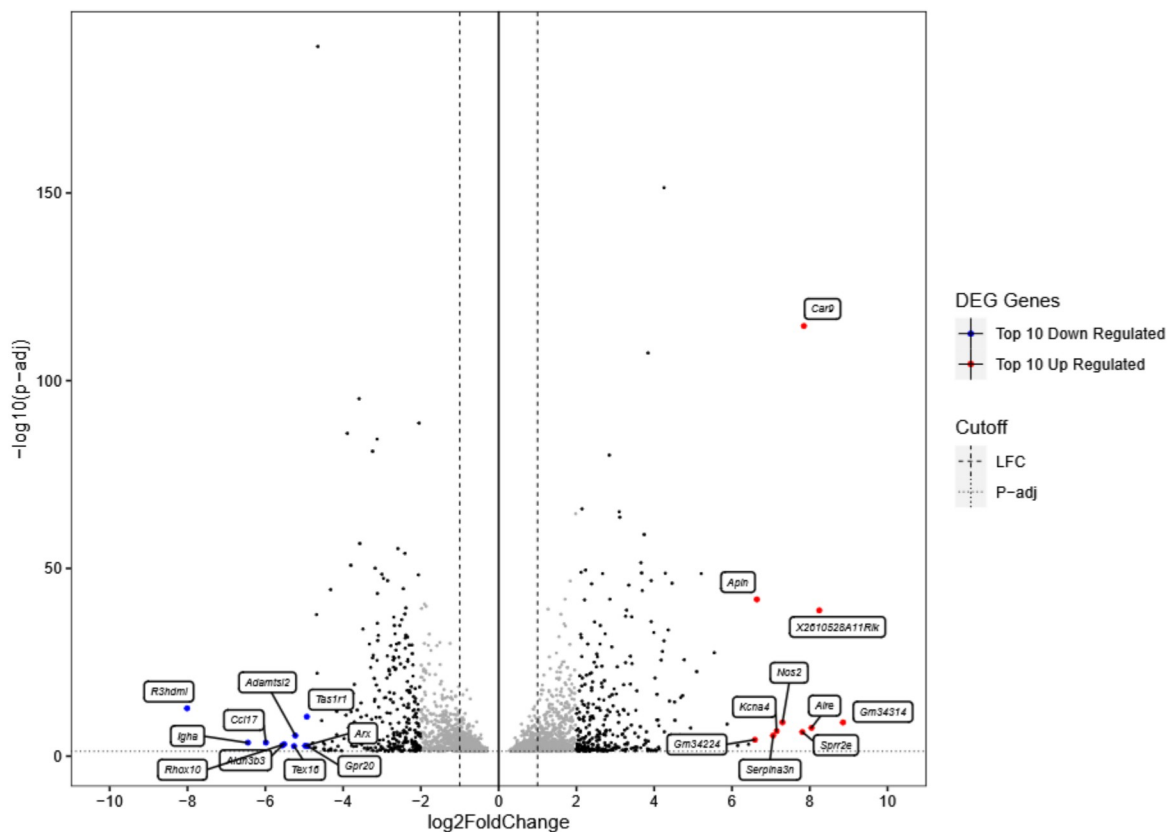


Figure 4.12: Volcano plot of the most affected genes after 96 hours. The plot reveals all higher regulated genes. Thereby, the TOP 10 gens for the positive and negative log2foldchange were visualized by color and naming. P-adjust < 0.05.

While another complete difference of gene expression within the normoxic group is observed within 144 hours, the genes within hypoxia remain mainly similar to 96 hours. The first myogenic differentiation markers as *Myh4* are present within N&H►Diff-N. (Fig.4.13)

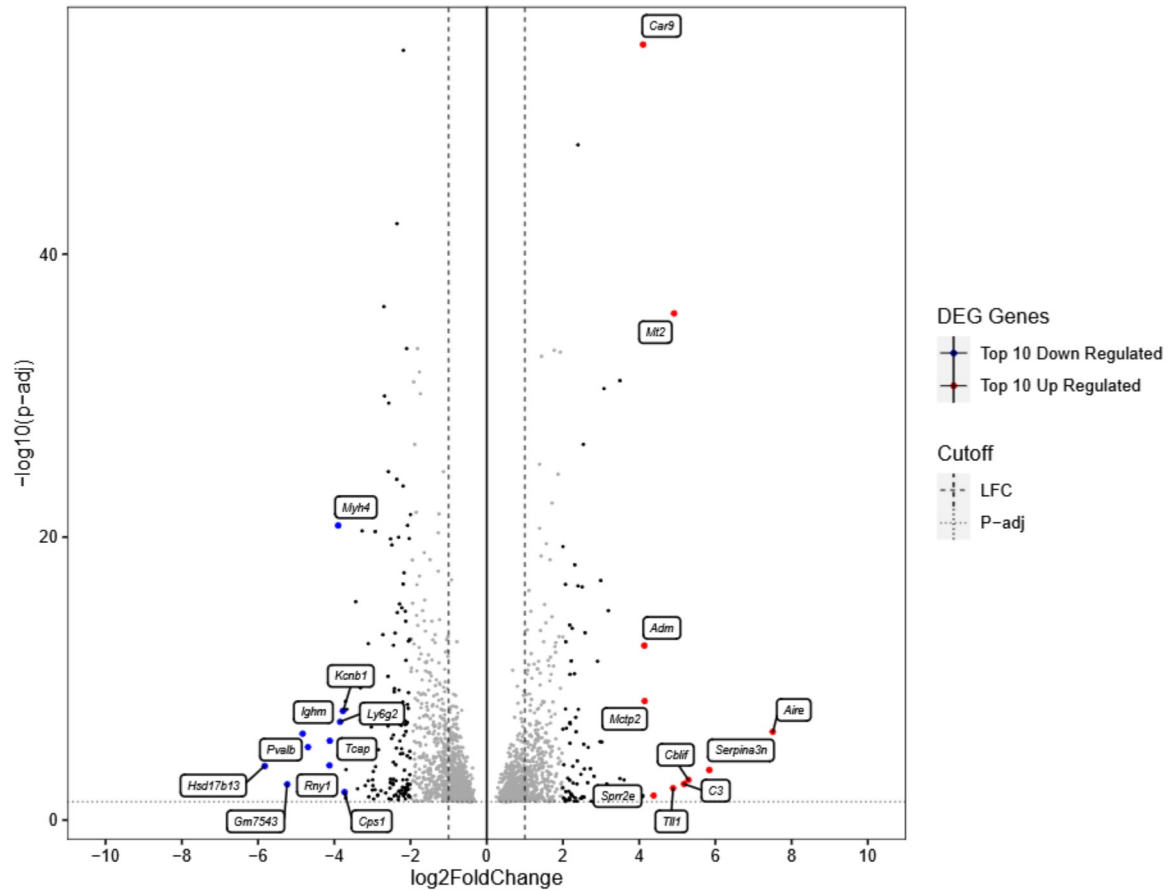


Figure 4.13: Volcano plot of the most affected genes after 144 hours. The plot reveals all higher regulated genes. Thereby, the TOP 10 gens for the positive and negative log2foldchange were visualized by color and naming. P-adjust < 0.05.

For further investigations, a hierarchical cluster analyses (HCA) of the top 50 differentially expressed genes out of 177, was performed, showing a clear separation of essential (increased expression over the time) or inhibitory (decrease over the time) myogenic genes (Fig. 4.14).

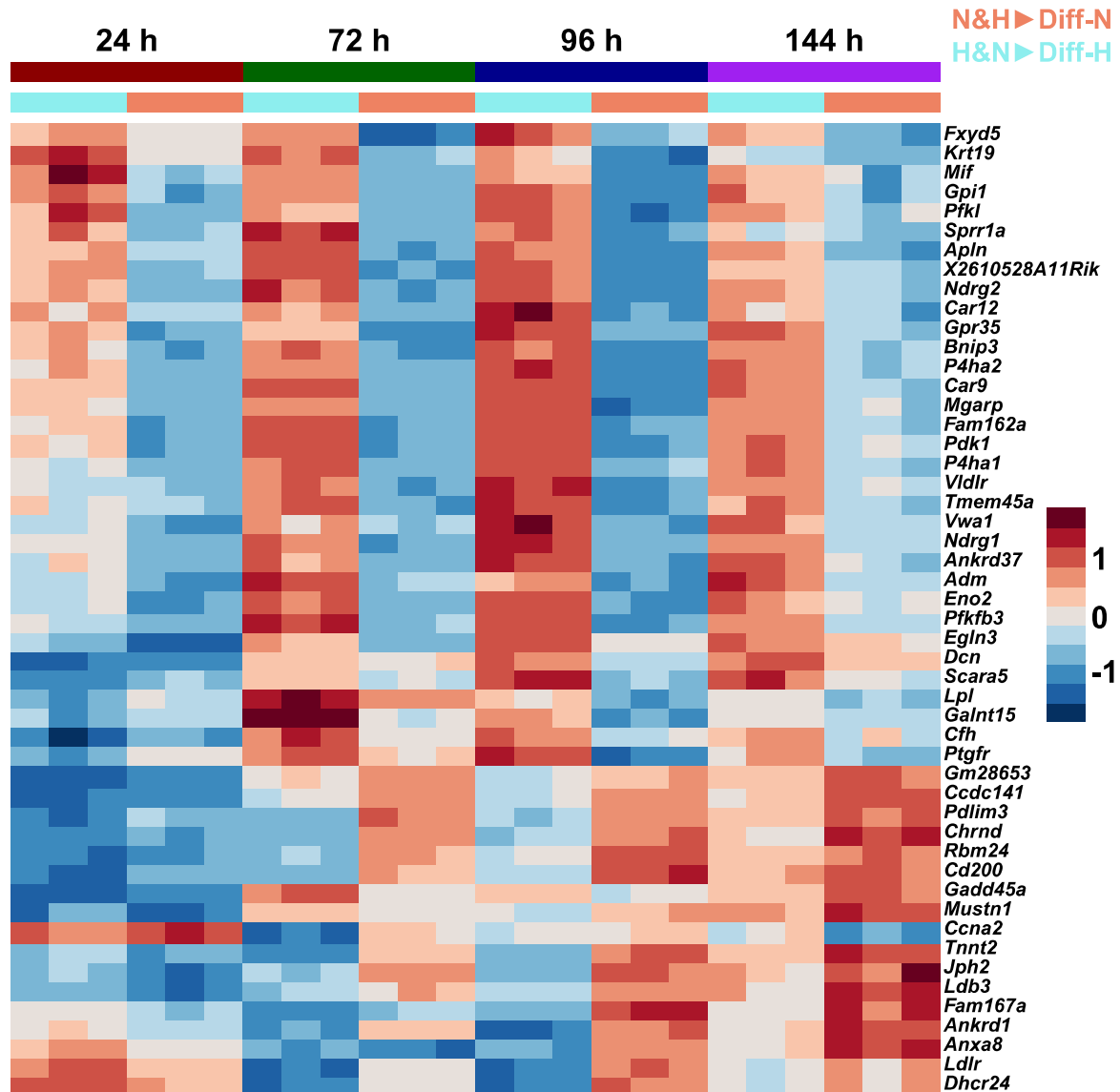


Figure 4.14: Hierarchical cluster analysis of the top 50 of 177 genes continuously differentially regulated genes. Positive value indicates a high expression (red), negative value a downregulation of the gene (blue). Adopted and modified from Pircher et al. (98).

Based on the HCA, 9 subjective promising genes were extrapolated. While the four genes, including *Adm*, *Apln*, *Car9* and *Gpr35* are constantly expressed during hypoxia, *Scara5* and the *prostaglandin F receptor gene (Ptgfr)* show initially higher expression within normoxia and show a switch of expression after 72 hours within both groups.

Other genes such as *Ankyrin repeat domain 1 (Ankrd1)* and *LIM domain binding 3 (Ldb3)* are initially upregulated in hypoxia, but they all show a switch of expression at 72 hours, indicating a possible adjustment within the time period between 24h and 72h. The remaining gene, *Actine-associated LIM protein (Pdlim3)* has a higher expression within normoxia (Fig. 4.15).

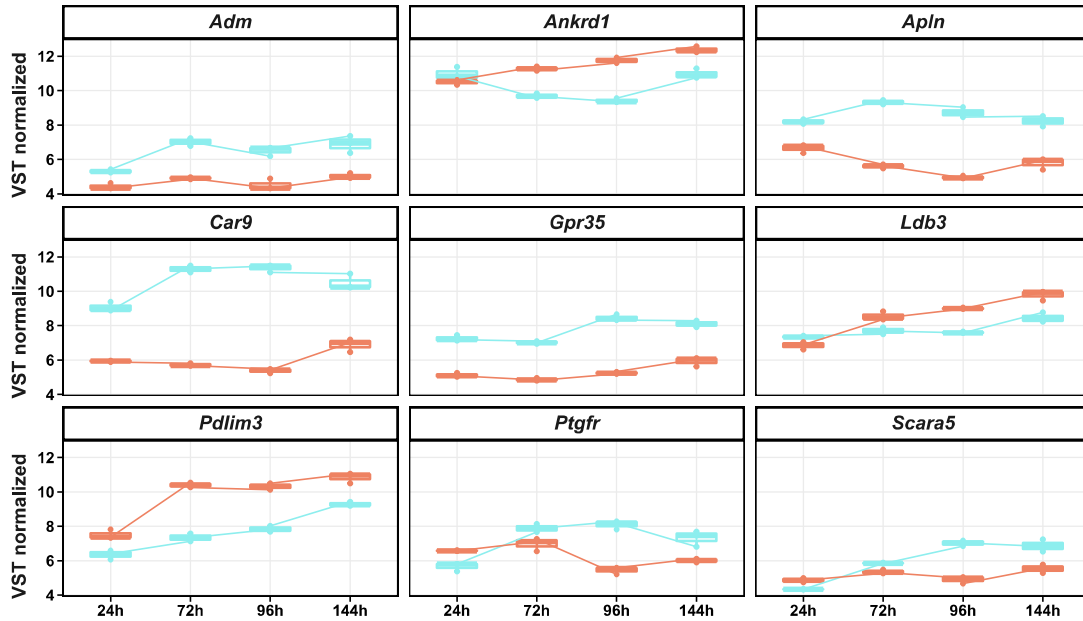


Figure 4.15: Expression of the 15 selected genes over 144 hours within normoxic (red) and hypoxic (blue) conditions was assessed and immediately compared. Genes are sorted alphabetically. Value refers to VST (variance stabilizing transformation) normalized. Adopted and modified from Pircher et al. (98).

Chapter 5

Discussion

Although muscle-specific stem cells are frequently exposed to hypoxic micro-environments, for example during development and regeneration (15), a longer period of hypoxia within skeletal muscles leads to severe physiological consequences, ranging from a loss of muscle function to necrosis (84). Ischemic injuries result from any interruption of blood supply, including arterial embolism, prolonged arterial clamping during, traumatic injury or vessel destruction, as well as acute atherosclerotic thrombosis and critical limb ischemia, usually caused by atherosclerotic plaques blocking the blood vessels (13). Worldwide, over 200 million people suffer from peripheral arterial disease (PAD), with a spectrum of symptoms from none to severe (111). Moreover, muscle atrophy and weakness are observed in several chronic diseases associated with hypoxemia (low arterial O₂ pressure), such as chronic obstructive pulmonary disease (COPD) and heart failure (112, 113). Therefore, the investigation in hypoxic effects on skeletal muscle cells is epidemiologically crucial, since not only orthopedic patients are affected.

Currently, skeletal muscle stem cells are seen as promising therapies for human muscle diseases (114, 115, 116). Several attempts to use satellite cell-derived myoblasts via intramuscular transplantation as therapeutic approach for degenerative muscle diseases have been made (117, 118, 119, 120, 121). For further investigations into new stem cell therapies, it is necessary to have precise comprehension of skeletal cell regulation during muscle repair. Thus, the aim of study was to investigate the interaction between hypoxic conditioned (2% O₂) and standardized ("normoxic", 21% O₂) cultured myoblasts to imitate realistic conditions and to find promising candidate genes,

regulated by hypoxia and differentiation within the mixed myoblast groups.

5.1 Long-Term Hypoxia Has No Significant Impact on Myoblast Morphology or Proliferation but Leads to Reduced Myogenesis

As shown in the results, hypoxia has no impact on the cellular area of the myoblasts. However, a slightly rounder cell phenotype within the hypoxic group (N&H►Diff-H) was visible, mainly due to the differences within the different dimensions of the myoblasts, represented by the aspect ratio. Within the RNA-sequencing a differences within the regulation of several cadherins, including cadherin 2 (CDH2), between N&H►Diff-H and N&H►Diff-N from 24h upwards (Table S1 from Pircher et al. (98)) was observed. This suggests, that the changes in the aspect ratio and the reduced myoblast fusion under hypoxic conditions are, at least partially, dependent on the expression of hypoxia-sensitive cadherin genes.

Conformational changes in cell membrane are involved in the cellular fusion process (122) and therefore morphological changes of myoblasts might have an impact on myoblast fusion, independently of the regulation of myogenic transcription factors. Cell fusion can occur in different ways, including fusion of the cell membranes, mostly accomplished by specific membrane proteins, pulling each membrane together through their conformational changes (122).

Myoblast differentiation during mammalian somitogenesis depends on the so-called community effect. It describes, that newly formed somites, must be surrounded by a minimum of 30-40 similar cells to differentiate (123). Additionally, for stable expression of myogenic factors, the presence of the adhesion molecules, as the plasma membrane bound N-cadherin (124) and the accumulation of CDKN1A and CDKN1B, involved in cell cycle withdraw (125, 126, 127), are necessary. Bensaid et al. already reported morphological changes in myotubes, due to a significant reduction in myotube diameter at 4% O₂ (128). However, they did not check for morphological changes prior to myoblast fusion. Therefore, to my knowledge, this is the first study including morphological changes of myoblasts in hypoxia.

An increased proliferation of mouse satellite cells (42) or human primary myoblasts

(43) within short-term hypoxia at 2% O₂ was shown, while long-term hypoxia revealed an adjustment of proliferation between normoxic and hypoxic conditions (43). Contrary to the myoblast proliferation, severe hypoxia (< 1% O₂) leads to the arrest of myogenic regulation factors necessary for differentiation (38). This thesis demonstrated similar results. An oxygen level of 2% O₂ over a period of 4 days resulted in reduced myoblast formation.

It is also important to analyze short-term hypoxic exposure, as for example during the period between restored blood flow and sufficient oxygenation within the tissue. This temporary hypoxic exposure showed similar results as long-term hypoxia. A decreased number and area of myotubes in the N►Diff-H group were observed, indicating that myoblasts adjust very quickly to hypoxia, including an inhibition of differentiation. Additionally, this thesis data showed that hypoxic differentiation of hypoxic preconditioned myoblasts (H►Diff-H), also lead to a reduction in myotube size and number by 40-60%. Even within normoxia (H►Diff-N), this downregulation of hypoxic preconditioned myotube size and number is present, indicating that the described negative effect above is largely irreversible.

The reduction of myogenesis under hypoxic conditions is multimodal, consisting of reduced fusion on one side and subsequent cell death due to energy restriction on the other side. Myoblast fusion is highly dependent on available energy sources such as adenosine triphosphate (ATP), an organic compound that provides energy to drive cellular processes and is necessary for muscle contraction (129). During the ischemic period, the synthesis of ATP is impaired, even though the skeletal muscle cells are able to adapt ATP utilization (130). Noteworthy, Dehne et al. showed a higher ability to maintain ATP levels and turnover within myoblasts, when compared to myotubes (67), confirming that myoblasts mainly depend on glycolytic energy production (131), whereas myotubes have an increased aerobic oxidation of fatty acids (132).

5.2 Hypoxia Leads to Increased Synergy between Hypoxia- and Normoxia-Cultured Myoblasts

After an ischemic injury, regeneration process can be activated (87, 88). However, to continue the regeneration process, recovery of blood flow in the affected injury area (89)

and migration of the satellite cells towards (re-)oxygenated tissue (133) is necessary. Therefore, under realistic conditions, it is more likely that not only normoxic myoblasts are present during regeneration, but also myoblasts that are affected by hypoxic stress. Similar interactions of myoblasts/satellite cells occur after intramuscular satellite cells transplantation, as shown by a novel therapy approach for ischemic muscle injuries (134, 135, 136). This thesis mainly focuses on the interaction between normoxic and hypoxic precultured myoblasts during fusion process in normoxic and hypoxic environments, mimicking physiological conditions. Regardless of the environmental exposure, both mixed groups (N&H►Diff-H and N&H►Diff-N) showed a smaller total number and area of myotubes compared to the normoxic group (N►Diff-N)(Fig. 4.5). However, both groups revealed a greater relative myotube size, suggesting hypertrophy as the leading mechanism in mixed myotube fusion. Thereby fewer, but larger myotubes are formed, which seems to depend on the direct fusion of normoxic and hypoxic preconditioned myoblasts, suggesting a synergistic effect of both groups.

5.3 Hypoxic Transcriptional Changes Are Partially Reversible during Myogenic Differentiation

After 48 hours of moderate hypoxia exposure (11.2%) on skeletal muscle cells, up-regulation of hypoxic related proteins have been reported, indicating hypoxic adjustment (137). This thesis revealed similar results, as transcriptional changes are already present between 24 and 72 hours of myogenic differentiation within hypoxia. The PCA shown in Fig. 4.7 [A], visualized the first separation between hypoxic (N&H►Diff-H) and normoxic mixed myoblast group (N&H►Diff-N) between 24 and 72 hours. Additionally, the proximity of N&H►Diff-H at 144h (Fig.4.7 [A], circles) and N&H►Diff-N at 72 hours (Fig.4.7 [A], triangles) supports the downregulated myogenic potential within 2% O₂ compared to normoxia.

After hypoxic damage, skeletal muscle repair is directly induced. It consists of three overlapping phases, starting with the destruction phase. Thereby, inflammation processes are induced by activating pro-inflammatory cytokines (138) and recruiting neutrophils, leading to nitric oxide (NO) mediated cell lysis in the damaged area (139) and finally results in muscle damage and atrophy (138). The hallmarks in Fig. 4.8 [B], exem-

plary reflect the repair process of skeletal muscle cells over the different time periods. The inflammatory response plays an important physiological role in adaptive remodeling of skeletal muscle tissue, initially presenting after 72 hours of hypoxia, by expressing IFA, IFG, IL2-STAT5 and TNFA hallmarks (Fig.4.8 [B]). Prostaglandin (PG) is part of the inflammatory process and has been implicated in multiple stages of myogenesis *in vitro*, including proliferation, differentiation (140), myoblast survival (141) and fusion (142). Additionally, prostaglandin 2 alpha (PGF2a) has been shown to be involved in post fusion myotube growth, as a direct stimulator of PI3K/ERK/mTOR pathway in skeletal myotubes (143). Within the hierarchical cluster analyses of this thesis, a PG receptor (*Ptgfr*) expression within the N&H►Diff-H group at 96 hours, was observed. It indicates its involvement within the inflammatory response of hypoxic myoblasts. Additionally, *Prostaglandin E Synthase 3 (Ptges3)* and *Prostaglandin Synthase 3 Like (Ptges3l)* were identified as novel candidates, involved in oxygen dependent hypertrophy.

After 96 hours of hypoxia, *Nos2* upregulation was denoted by the upregulation of inducible NO synthase (iNOS) encoding. iNOS has been described during embryonic muscle development (144), whereas in the adult, it only occurs during muscle regeneration. It has a critical role in the modulation of inflammatory response during regeneration (108).

After the inflammation, repair phase follows. Satellite cells are activated and in turn start to proliferate, differentiate and to form new multinucleated muscle fibers (145, 146). Additionally, vascularization is promoted by the release of VEGF (147). During this phase, the differences between the two oxygen levels are clearly visible in the GSEA. At 2% O₂, the response to *E2F* targets in N&H is much higher than at 21% O₂ (Fig.4.8 [B]), indicating a downregulation of myoblast proliferation and differentiation process, since *E2F* is essential for the suppression of proliferative transcription programs and the exit of myoblasts from the cell cycle (148). However, 2% O₂ was not enough to entirely prevent myoblast differentiation. Although hypoxia showed an impact onto myogenesis, *mTOR1* signaling, involved in myoblast proliferation and differentiation (54), was still present within N&H►Diff-H.

In 2019, Sakamoto et al. discovered a novel gene expressed in myogenic satellite cells. *R3h domain containing-like (R3hdml)* showed to be particularly important for their proliferation and differentiation processes. It is not only expressed during skeletal muscle development, but also in the process of regenerating after injury. They especially

indicated an interaction of IGF-1/AKT signaling with the *R3hdml*, due to pathway down-regulation within *R3hdml* KO skeletal muscle (110). The PI3-AKT-signalling pathway is already known to participate in myogenic differentiation and is downregulated during oxygen deprivation (55). The observed downregulation of *R3hdml* in the N&H►Diff-H group after 144h, suggests a possible mechanism of the downregulation, triggered by PI3-AKT-signalling pathway. However, a more detailed functional investigation is necessary to confirm that assumption.

Several more transcripts involved in hypoxic adjustment of myoblasts were shown in the analysis of gene expression levels between hypoxic and normoxic environment. One of them is *Apln*, upregulated after 24 hours within N&H►Diff-H and reaching its maximum after 72 hours (Fig. 4.15). The gene encoding Apelin, an endogenous ligand for the G protein-coupled receptor APJ, showed to be upregulated over all of the time points in hypoxia. In contrast to the skeletal muscle, where it has not been reported so far, a low baseline level of Apelin expression and secretion in cardiomyocytes is known (149). The same study additionally showed that *Apln* expression increase, if cardiac myocytes were exposed to hypoxia of 2% O₂. After 24h, induction of *Apln* was severalfold higher in comparison to the known HIF target gene *Adm* and they were able to provide strong evidence for the role of HIF1A in the transcriptional regulation of *Apln* (149). In synopsis with this thesis's results, a similar mechanism during the differentiation process of skeletal myoblasts is assumed. Moreover, *Apln* is associated with age-related muscle wasting (sarcopenia) in rodents and humans (150), leading to the hypothesis, that regulation of *Apln* is, at least partially, oxygen-driven, as the oxidative capacity of skeletal muscle cells reduces during ageing (151).

On the other side, gene expression analyses revealed upregulated genes within the normoxic group (N&H►Diff-N) that were not present at 2% O₂. One of them is *Low density lipoprotein receptor gene (Ldlr)*, which was mainly expressed between 96 and 144 hours. Prior studies showed its involvement in reduction of skeletal muscle differentiation due to vitamin K (152). Other genes were *Pdlim3*, encoding for the actin-associated LIM protein, and with *Ldb3*, encoding for Z-band alternatively spliced PDZ-motif protein (*Ldb3*; Cypher; ZASP), both upregulated after 72 hours within N&H►Diff-N. Both genes are containing LIM domains, which play a role in the process of myogenesis (153). Prior studies already confirmed a dramatic increase in C2C12 differentiation by *Pdlim3* expression (154). Recently, Yin et al. observed that p38 (MAPK14) can be activated by

Pdlim3 during myogenesis, providing a reason for the influence on the myoblast differentiation (155). *Ldb3* is known for the interaction with skeletal muscle actin, regulating the remodelling of the actin cytoskeleton in striated muscle (156). Additionally, it has been proposed that the cytoplasmic region of the protein is involved in the interaction with *Ankyrin repeat domain 2* (*Ankrd2*) (157), a member of the Muscle ankyrin repeat protein (MARPs), such as CARP encoded by *Ankrd1* gene.

Even though *Ankrd1* is mainly associated with cardiac muscle and *Ankrd2* is the most abundant MARP in human skeletal muscle (158), expression of *Ankrd1* in skeletal muscle fibers could be confirmed. Thereby, it was preferably expressed in type one skeletal muscle fibers (159) and shown to be involved in transduction of stretch-induced signaling due to its titin-association (160). During myogenic differentiation, *Ankrd1* is transferred from the nucleus to the cytoplasm (161). Interestingly, in 2015 a study revealed that *Ankrd1* is upregulated by nuclear factor kappa-light-chain-enhancer of activated B-cells (NF- κ B) activation, due to either TNFA upregulation or increased level of ROS as during hypoxia (162). In this case, an upregulation of *Ankrd1* within the hypoxic group was expected.

Surprisingly, next to *Ankrd1*, *troponin T2* (*Tnnt2*) and *Junctophilin2* (*Jph2*) were expressed within the N&H►Diff-N, with the highest extent after 144h. Both genes are known as cardiac isoforms (163, 164), which in particular circumstances can be expressed in skeletal muscle as well. *Jph2* mainly plays a key role in cardiomyocyte development and differentiation (165) and has been shown to induce skeletal myotube hypertrophy, if *Jph2*-S165F (166) or *Jph2*-Y141H mutation (167) are present. *Tnnt2* is physiologically transiently expressed in embryonic and neonatal skeletal muscle, including both slow and fast fiber dominant muscles (168, 169).

The *X2610528A11Rik*, showed a great impact onto hypoxic myoblasts and was present within the 177 most influential genes. The gene was initially discovered in 2003 during the Riken mouse genome encyclopedia project in Japan, by comprehensive sequencing of the mouse genome. Until now it is not known, which function the protein has or how it is regulated.

Another promising gene is the *Potassium Voltage-Gated Channel Subfamily A Member 4* (*Kcna4*), coding for the Kv1.4-channel, revealing an upregulation in N&H►Diff-H after 96 hours. The voltage-gated potassium channel is very well known within cortical pyramidal neurons, necessary for fast repolarization phase of action

potential and with a central role in long-term plasticity, essential for learning and memory (100). It is possible that *Kcna4* is involved in myoblast adaption onto hypoxia, similar to neuron plasticity. However further investigations are necessary.

Taken together, a partial delay of myogenic differentiation within N&H►Diff-H was observed within the period of 6 days, which seems to be partially reversible. However, as transcriptional responses to hypoxia is relatively fast *in vitro*, further time points and longer observation periods should be evaluated in further experiments. However, very promising candidate genes were found that are involved in hypoxic-related myogenesis and especially myotube hypertrophy.

5.4 Within Hypoxia, Skeletal Muscle Hypertrophy Shows Parallels to Cancer Cell Behavior

During hypertrophy, increased glycolysis and metabolic reprogramming of the skeletal muscle cells, similar to those in cancer cells (170) have been reported (171). This thesis revealed several cancer-associated genes, which were upregulated within the N&H►Diff-H group, sustaining a similarity between skeletal muscle cell and cancer cells. One of the most studied gene is *Car9*. It is known for its expression in solid tumors, such as the renal clear cell carcinoma (172). Thereby it is principally related to tumor hypoxia. This thesis revealed an upregulation of *Car9* after 24 hours within the hypoxic mixed myoblast group (N&H►Diff-H) and a remaining upregulation over all further time points. Just upstream to the transcription initiation site of *Car9* promoter, an HRE binding site is localized (172), which appears to be epigenetically active in zebrafish muscles in response to hypoxia (173).

Another tumor associated gene observed during prolonged hypoxia in N&H►Diff-H was *Scavenger Receptor Class A Member 5 (Scara5)*. It is associated with tumor suppressor character at liver (174), lung (175) and breast cancer (176), as well as osteosarcoma (177), but has never been mentioned with skeletal muscle cells so far. A correlation to hypoxia was firstly observed by Yu et al. They showed negative correlation of *Scara5* with *VEGF*, leading to a downregulation of angiogenesis. Additionally, they observed decreased phosphorylation levels of AKT and Mitogen-Activated Protein Kinase 3/1 (ERK1/2), both known to be also involved in myogenic differentiation (176). It is possible that this mechanism also occurs within myoblasts in not tumor associated hypoxia, but caused by environmental oxygen deprivation.

It is notable, that many of the detected genes in this thesis interact with the PI3K/ AKT/ mTOR pathway. Likewise does *Gpr35*, by activation of ERK1/2 (102). Until now, no link of *Gpr35* to muscle cells was observed, so it is not conclusively proven, if this process occurs within skeletal muscle cells as well. However, since a continuous upregulation within N&H►Diff-H, with a maximum at 96h was observed, it can be assumed, that the known regulation is transferable to myoblasts. Nevertheless, to confirm the assumption, more precise genomic analyzes are necessary.

Noteworthy, within N&H►Diff-H, an upregulation of KRAS-signaling, as a response to hypoxia was observed. *KRAS* is a proto-oncogene and part of the RAS/MAPK path-

way, involved in cellular proliferation (178). It is commonly known in oncology, due to the association with colon, pancreatic and lung cancer (179), but was never linked to myogenic differentiation in response to hypoxia before. Nevertheless, interaction between *KRAS* and hypoxia have already been described by Kikuchi et al., showing an effect on the regulation of HIF1A translation (180). It is possible, that similar interactions within hypoxic exposure of skeletal muscle cells take place. For confirmation however, deeper investigations in the gene are necessary.

In the end, as suggested above, the commonly known mTOR-pathway, popular for its major impact onto hypoxic adjustment within skeletal muscle and cancer cells, was detected in this thesis. Both cell types reveal an increased IGF-AKT1-mTOR1 and reduced myostatin signaling (170).

Chapter 6

Outlook

Taken together, the interaction of hypoxic and normoxic myoblasts leads to an overall decrease in total number and area of myoblasts, but results in a higher myotube hypertrophy. This hypoxia-dependent skeletal muscle hypertrophy shows, several similarities to cancer cell adjustment within hypoxia, indicating a similar reprogramming strategies within skeletal muscle cells and cancer cells within oxygen deprivation. Nevertheless, to finally confirm this assumption, further loss-and gain-of-function experiments with the described promising candidate genes are necessary.

Bibliography

- [1] J. Chal and O. Pourquié. Making muscle: skeletal myogenesis in vivo and in vitro. *Development*, 144(12):2104–2122, 2017.
- [2] David Horst, Svetlana Ustanina, Consolato Sergi, Gregor Mikuz, Herbert Juergens, Thomas Braun, and Eugene Vorobyov. Comparative expression analysis of pax3 and pax7 during mouse myogenesis. *International journal of developmental biology*, 50(1):47–54, 2003.
- [3] Anthony Otto, Corina Schmidt, and Ketan Patel. Pax3 and pax7 expression and regulation in the avian embryo. *Anatomy and embryology*, 211(4):293–310, 2006.
- [4] Robert Van Horn and Michael T Crow. Fast myosin heavy chain expression during the early and late embryonic stages of chicken skeletal muscle development. *Developmental biology*, 134(2):279–288, 1989.
- [5] Frédéric Relaix, Didier Rocancourt, Ahmed Mansouri, and Margaret Buckingham. A pax3/pax7-dependent population of skeletal muscle progenitor cells. *Nature*, 435(7044):948–953, 2005.
- [6] H. Takayama, W. J. La Rochelle, M. Anver, D. E. Bockman, and G. Merlino. Scatter factor/hepatocyte growth factor as a regulator of skeletal muscle and neural crest development. *Proc Natl Acad Sci U S A*, 93(12):5866–71, 1996.
- [7] S. B. Chargé and M. A. Rudnicki. Cellular and molecular regulation of muscle regeneration. *Physiol Rev*, 84(1):209–38, 2004.
- [8] N. Itoh, T. Mima, and T. Mikawa. Loss of fibroblast growth factor receptors is necessary for terminal differentiation of embryonic limb muscle. *Development*, 122(1):291–300, 1996.

- [9] D. J. Milasincic, M. R. Calera, S. R. Farmer, and P. F. Pilch. Stimulation of c2c12 myoblast growth by basic fibroblast growth factor and insulin-like growth factor 1 can occur via mitogen-activated protein kinase-dependent and -independent pathways. *Mol Cell Biol*, 16(11):5964–73, 1996.
- [10] E. Vasyutina, D. C. Lenhard, and C. Birchmeier. Notch function in myogenesis. *Cell Cycle*, 6(12):1451–4, 2007.
- [11] A. R. Greenbaum, P. J. Etherington, S. Manek, D. O'Hare, K. H. Parker, C. J. Green, J. R. Pepper, and C. P. Winlove. Measurements of oxygenation and perfusion in skeletal muscle using multiple microelectrodes. *J Muscle Res Cell Motil*, 18(2):149–59, 1997.
- [12] Z. Yun, Q. Lin, and A. J. Giaccia. Adaptive myogenesis under hypoxia. *Mol Cell Biol*, 25(8):3040–55, 2005.
- [13] Lars Norgren, William R Hiatt, John A Dormandy, Mark R Nehler, Kenneth A Harris, and F Gerry R Fowkes. Inter-society consensus for the management of peripheral arterial disease (tasc ii). *Journal of vascular surgery*, 45(1):S5–S67, 2007.
- [14] P. S. Zammit, J. P. Golding, Y. Nagata, V. Hudon, T. A. Partridge, and J. R. Beauchamp. Muscle satellite cells adopt divergent fates: a mechanism for self-renewal? *J Cell Biol*, 166(3):347–57, 2004.
- [15] K. Parmar, P. Mauch, J. A. Vergilio, R. Sackstein, and J. D. Down. Distribution of hematopoietic stem cells in the bone marrow according to regional hypoxia. *Proc Natl Acad Sci U S A*, 104(13):5431–6, 2007.
- [16] W. Liu, Y. Wen, P. Bi, X. Lai, X. S. Liu, X. Liu, and S. Kuang. Hypoxia promotes satellite cell self-renewal and enhances the efficiency of myoblast transplantation. *Development*, 139(16):2857–65, 2012.
- [17] S. Ciciliot and S. Schiaffino. Regeneration of mammalian skeletal muscle. basic mechanisms and clinical implications. *Curr Pharm Des*, 16(8):906–14, 2010.
- [18] C Florian Bentzinger, Julia von Maltzahn, Nicolas A Dumont, Danny A Stark, Yu Xin Wang, Kevin Nhan, Jérôme Frenette, DDW Cornelison, and Michael A

- Rudnicki. Wnt7a stimulates myogenic stem cell motility and engraftment resulting in improved muscle strength, 2014.
- [19] J Manuel Hernández-Hernández, Estela G García-González, Caroline E Brun, and Michael A Rudnicki. The myogenic regulatory factors, determinants of muscle development, cell identity and regeneration. In *Seminars in cell & developmental biology*, volume 72, pages 10–18. Elsevier, 2017.
- [20] C Florian Bentzinger, Yu Xin Wang, and Michael A Rudnicki. Building muscle: molecular regulation of myogenesis, 2012.
- [21] L. Cicchillitti, V. Di Stefano, E. Isaia, L. Crimaldi, P. Fasanaro, V. Ambrosino, A. Antonini, M. C. Capogrossi, C. Gaetano, G. Piaggio, and F. Martelli. Hypoxia-inducible factor 1-alpha induces mir-210 in normoxic differentiating myoblasts. *J Biol Chem*, 287(53):44761–71, 2012.
- [22] M. Horak, J. Novak, and J. Bienertova-Vasku. Muscle-specific microRNAs in skeletal muscle development. *Dev Biol*, 410(1):1–13, 2016.
- [23] S. W. Lee, J. Yang, S. Y. Kim, H. K. Jeong, J. Lee, W. J. Kim, E. J. Lee, and H. S. Kim. MicroRNA-26a induced by hypoxia targets hdac6 in myogenic differentiation of embryonic stem cells. *Nucleic Acids Res*, 43(4):2057–73, 2015.
- [24] John J McCarthy, Karyn A Esser, and Francisco H Andrade. MicroRNA-206 is over-expressed in the diaphragm but not the hindlimb muscle of mdx mouse. *American Journal of Physiology-Cell Physiology*, 293(1):C451–C457, 2007.
- [25] J. F. Chen, Y. Tao, J. Li, Z. Deng, Z. Yan, X. Xiao, and D. Z. Wang. microRNA-1 and microRNA-206 regulate skeletal muscle satellite cell proliferation and differentiation by repressing pax7. *J Cell Biol*, 190(5):867–79, 2010.
- [26] B. K. Dey, J. Gagan, and A. Dutta. mir-206 and -486 induce myoblast differentiation by downregulating pax7. *Mol Cell Biol*, 31(1):203–14, 2011.
- [27] J. F. Chen, E. M. Mandel, J. M. Thomson, Q. Wu, T. E. Callis, S. M. Hammond, F. L. Conlon, and D. Z. Wang. The role of microRNA-1 and microRNA-133 in skeletal muscle proliferation and differentiation. *Nat Genet*, 38(2):228–33, 2006.

- [28] John J McCarthy, Karyn A Esser, Charlotte A Peterson, and Esther E Dupont-Versteegden. Evidence of myomir network regulation of β -myosin heavy chain gene expression during skeletal muscle atrophy. *Physiological genomics*, 39(3): 219–226, 2009.
- [29] H. W. Kim, H. K. Haider, S. Jiang, and M. Ashraf. Ischemic preconditioning augments survival of stem cells via mir-210 expression by targeting caspase-8-associated protein 2. *J Biol Chem*, 284(48):33161–8, 2009.
- [30] M. V. Gustafsson, X. Zheng, T. Pereira, K. Gradin, S. Jin, J. Lundkvist, J. L. Ruas, L. Poellinger, U. Lendahl, and M. Bondesson. Hypoxia requires notch signaling to maintain the undifferentiated cell state. *Dev Cell*, 9(5):617–28, 2005.
- [31] T. Kitamura, Y. I. Kitamura, Y. Funahashi, C. J. Shawber, D. H. Castrillon, R. Kolipara, R. A. DePinho, J. Kitajewski, and D. Accili. A foxo/notch pathway controls myogenic differentiation and fiber type specification. *J Clin Invest*, 117(9):2477–85, 2007.
- [32] Alice E Chen, David D Ginty, and Chen-Ming Fan. Protein kinase a signalling via creb controls myogenesis induced by wnt proteins. *Nature*, 433(7023):317–322, 2005.
- [33] Ugo Borello, Barbara Berarducci, Paula Murphy, Lola Bajard, Viviana Buffa, Stefano Piccolo, Margaret Buckingham, and Giulio Cossu. The wnt/ β -catenin pathway regulates gli-mediated myf5 expression during somitogenesis. 2006.
- [34] J. von Maltzahn, C. F. Bentzinger, and M. A. Rudnicki. Wnt7a-fzd7 signalling directly activates the akt/mtor anabolic growth pathway in skeletal muscle. *Nat Cell Biol*, 14(2):186–91, 2011.
- [35] M. T. Veeman, J. D. Axelrod, and R. T. Moon. A second canon. functions and mechanisms of beta-catenin-independent wnt signaling. *Dev Cell*, 5(3):367–77, 2003.
- [36] F. Cirillo, G. Resmini, A. Ghioldi, M. Piccoli, S. Bergante, G. Tettamanti, and L. Anastasia. Activation of the hypoxia-inducible factor 1alpha promotes myogenesis through the noncanonical wnt pathway, leading to hypertrophic myotubes. *Faseb j*, 31(5):2146–2156, 2017.

- [37] L. Leroux, B. Descamps, N. F. Tojais, B. Seguy, P. Oses, C. Moreau, D. Daret, Z. Ivanovic, J. M. Boiron, J. M. Lamaziere, P. Dufourcq, T. Couffinhal, and C. Duplaa. Hypoxia preconditioned mesenchymal stem cells improve vascular and skeletal muscle fiber regeneration after ischemia through a wnt4-dependent pathway. *Mol Ther*, 18(8):1545–52, 2010.
- [38] A. Di Carlo, R. De Mori, F. Martelli, G. Pompilio, M. C. Capogrossi, and A. Germani. Hypoxia inhibits myogenic differentiation through accelerated myod degradation. *J Biol Chem*, 279(16):16332–8, 2004.
- [39] J. W. Schneider, W. Gu, L. Zhu, V. Mahdavi, and B. Nadal-Ginard. Reversal of terminal differentiation mediated by p107 in rb^{-/-} muscle cells. *Science*, 264(5164):1467–71, 1994.
- [40] B. G. Novitch, G. J. Mulligan, T. Jacks, and A. B. Lassar. Skeletal muscle cells lacking the retinoblastoma protein display defects in muscle gene expression and accumulate in s and g2 phases of the cell cycle. *J Cell Biol*, 135(2):441–56, 1996.
- [41] Tamara Pircher, Henning Wackerhage, Attila Aszodi, Christian Kammerlander, Wolfgang Böcker, and Maximilian Michael Saller. Hypoxic signaling in skeletal muscle maintenance and regeneration: a systematic review. *Frontiers in Physiology*, 12:684899, 2021.
- [42] L. Urbani, M. Piccoli, C. Franzin, M. Pozzobon, and P. De Coppi. Hypoxia increases mouse satellite cell clone proliferation maintaining both in vitro and in vivo heterogeneity and myogenic potential. *PLoS One*, 7(11):e49860, 2012.
- [43] M. Koning, P. M. Werker, M. J. van Luyn, and M. C. Harmsen. Hypoxia promotes proliferation of human myogenic satellite cells: a potential benefactor in tissue engineering of skeletal muscle. *Tissue Eng Part A*, 17(13-14):1747–58, 2011.
- [44] L. A. Megeney, B. Kablar, K. Garrett, J. E. Anderson, and M. A. Rudnicki. Myod is required for myogenic stem cell function in adult skeletal muscle. *Genes Dev*, 10(10):1173–83, 1996.
- [45] R. N. Cooper, S. Tajbakhsh, V. Mouly, G. Cossu, M. Buckingham, and G. S. Butler-Browne. In vivo satellite cell activation via myf5 and myod in regenerating mouse skeletal muscle. *J Cell Sci*, 112 (Pt 17):2895–901, 1999.

- [46] D. D. Cornelison and B. J. Wold. Single-cell analysis of regulatory gene expression in quiescent and activated mouse skeletal muscle satellite cells. *Dev Biol*, 191(2):270–83, 1997.
- [47] M. Ogilvie, X. Yu, V. Nicolas-Metral, S. M. Pulido, C. Liu, U. T. Ruegg, and C. T. Noguchi. Erythropoietin stimulates proliferation and interferes with differentiation of myoblasts. *J Biol Chem*, 275(50):39754–61, 2000.
- [48] Y. Jia, N. Suzuki, M. Yamamoto, M. Gassmann, and C. T. Noguchi. Endogenous erythropoietin signaling facilitates skeletal muscle repair and recovery following pharmacologically induced damage. *Faseb j*, 26(7):2847–58, 2012.
- [49] K. Wang, C. Wang, F. Xiao, H. Wang, and Z. Wu. Jak2/stat2/stat3 are required for myogenic differentiation. *J Biol Chem*, 283(49):34029–36, 2008.
- [50] M. Kozakowska, M. Ciesla, A. Stefanska, K. Skrzypek, H. Was, A. Jazwa, A. Grochot-Przeczek, J. Kotlinowski, A. Szymula, A. Bartelik, M. Mazan, O. Yagensky, U. Florczyk, K. Lemke, A. Zebzda, G. Dyduch, W. Nowak, K. Szade, J. Stepniewski, M. Majka, R. Derlacz, A. Loboda, J. Dulak, and A. Jozkowicz. Heme oxygenase-1 inhibits myoblast differentiation by targeting myomirs. *Antioxid Redox Signal*, 16(2):113–27, 2012.
- [51] A. Jazwa, J. Stepniewski, M. Zamykal, J. Jagodzinska, M. Meloni, C. Emanuelli, A. Jozkowicz, and J. Dulak. Pre-emptive hypoxia-regulated ho-1 gene therapy improves post-ischaemic limb perfusion and tissue regeneration in mice. *Cardiovasc Res*, 97(1):115–24, 2013.
- [52] T. N. Stitt, D. Drujan, B. A. Clarke, F. Panaro, Y. Timofeyva, W. O. Kline, M. Gonzalez, G. D. Yancopoulos, and D. J. Glass. The igf-1/pi3k/akt pathway prevents expression of muscle atrophy-induced ubiquitin ligases by inhibiting foxo transcription factors. *Mol Cell*, 14(3):395–403, 2004.
- [53] Se-Jin Lee and Alexandra C McPherron. Regulation of myostatin activity and muscle growth. *Proceedings of the National Academy of Sciences*, 98(16):9306–9311, 2001.

- [54] S. Hauerslev, J. Vissing, and T. O. Krag. Muscle atrophy reversed by growth factor activation of satellite cells in a mouse muscle atrophy model. *PLoS One*, 9(6):e100594, 2014.
- [55] H. Ren, D. Accili, and C. Duan. Hypoxia converts the myogenic action of insulin-like growth factors into mitogenic action by differentially regulating multiple signaling pathways. *Proc Natl Acad Sci U S A*, 107(13):5857–62, 2010.
- [56] Maurice Hayot, Julie Rodriguez, Barbara Vernus, Gilles Carnac, Elise Jean, David Allen, Lucie Goret, Philippe Obert, Robin Candau, and Anne Bonnieu. Myostatin up-regulation is associated with the skeletal muscle response to hypoxic stimuli. *Molecular and cellular endocrinology*, 332(1-2):38–47, 2011.
- [57] L. A. Garcia, K. K. King, M. G. Ferrini, K. C. Norris, and J. N. Artaza. 1,25(oh)₂vitamin d₃ stimulates myogenic differentiation by inhibiting cell proliferation and modulating the expression of promyogenic growth factors and myostatin in c2c12 skeletal muscle cells. *Endocrinology*, 152(8):2976–86, 2011.
- [58] A. J. Majmundar, N. Skuli, R. C. Mesquita, M. N. Kim, A. G. Yodh, M. Nguyen-McCarty, and M. C. Simon. O₂ regulates skeletal muscle progenitor differentiation through phosphatidylinositol 3-kinase/akt signaling. *Mol Cell Biol*, 32(1):36–49, 2012.
- [59] Y. Li, Y. Wang, E. Kim, P. Beemiller, C. Y. Wang, J. Swanson, M. You, and K. L. Guan. Bnip3 mediates the hypoxia-induced inhibition on mammalian target of rapamycin by interacting with rheb. *J Biol Chem*, 282(49):35803–13, 2007.
- [60] B. G. Wouters and M. Koritzinsky. Hypoxia signalling through mtor and the unfolded protein response in cancer. *Nat Rev Cancer*, 8(11):851–64, 2008.
- [61] Z. Zhang, L. Zhang, Y. Zhou, L. Li, J. Zhao, W. Qin, Z. Jin, and W. Liu. Increase in hdac9 suppresses myoblast differentiation via epigenetic regulation of autophagy in hypoxia. *Cell Death Dis*, 10(8):552, 2019.
- [62] Z. Zhou and A. Bornemann. Mrf4 protein expression in regenerating rat muscle. *J Muscle Res Cell Motil*, 22(4):311–6, 2001.

- [63] A. A. Chakraborty, T. Laukka, M. Myllykoski, A. E. Ringel, M. A. Booker, M. Y. Tolstorukov, Y. J. Meng, S. R. Meier, R. B. Jennings, A. L. Creech, Z. T. Herbert, S. K. McBrayer, B. A. Olenchock, J. D. Jaffe, M. C. Haigis, R. Beroukhim, S. Signoretti, P. Koivunen, and Jr. Kaelin, W. G. Histone demethylase kdm6a directly senses oxygen to control chromatin and cell fate. *Science*, 363(6432):1217–1222, 2019.
- [64] J. H. Marxsen, P. Stengel, K. Doege, P. Heikkinen, T. Jokilehto, T. Wagner, W. Jelkmann, P. Jaakkola, and E. Metzen. Hypoxia-inducible factor-1 (hif-1) promotes its degradation by induction of hif-alpha-prolyl-4-hydroxylases. *Biochem J*, 381(Pt 3):761–7, 2004.
- [65] C. P. Bracken, M. L. Whitelaw, and D. J. Peet. The hypoxia-inducible factors: key transcriptional regulators of hypoxic responses. *Cell Mol Life Sci*, 60(7):1376–93, 2003.
- [66] H. Niemi, K. Honkonen, P. Korpisalo, J. Huusko, E. Kansanen, M. Merentie, T. T. Rissanen, H. Andre, T. Pereira, L. Poellinger, K. Alitalo, and S. Yla-Herttuala. Hif-1 alpha and hif-2alpha induce angiogenesis and improve muscle energy recovery. *Eur J Clin Invest*, 44(10):989–99, 2014.
- [67] N. Dehne, U. Kerkweg, T. Otto, and J. Fandrey. The hif-1 response to simulated ischemia in mouse skeletal muscle cells neither enhances glycolysis nor prevents myotube cell death. *Am J Physiol Regul Integr Comp Physiol*, 293(4):R1693–701, 2007.
- [68] A. Germani, A. Di Carlo, A. Mangoni, S. Straino, C. Giacinti, P. Turrini, P. Biglioli, and M. C. Capogrossi. Vascular endothelial growth factor modulates skeletal myoblast function. *Am J Pathol*, 163(4):1417–28, 2003.
- [69] K. M. Gutpell and L. M. Hoffman. Vegf induces stress fiber formation in fibroblasts isolated from dystrophic muscle. *J Cell Commun Signal*, 9(4):353–60, 2015.
- [70] C. Wang, W. Liu, Z. Liu, L. Chen, X. Liu, and S. Kuang. Hypoxia inhibits myogenic differentiation through p53 protein-dependent induction of bhlhe40 protein. *J Biol Chem*, 290(50):29707–16, 2015.
- [71] K. M. Sinha, C. Tseng, P. Guo, A. Lu, H. Pan, X. Gao, R. Andrews, H. Eltzschig, and J. Huard. Hypoxia-inducible factor 1 alpha (hif-1 alpha) is a major determinant

- in the enhanced function of muscle-derived progenitors from mrl/mpj mice. *Faseb j*, page fj201801794R, 2019.
- [72] K. L. Flann, C. R. Rathbone, L. C. Cole, X. Liu, R. E. Allen, and R. P. Rhoads. Hypoxia simultaneously alters satellite cell-mediated angiogenesis and hepatocyte growth factor expression. *J Cell Physiol*, 229(5):572–9, 2014.
- [73] L. Xie, A. Yin, A. S. Nichenko, A. M. Beedle, J. A. Call, and H. Yin. Transient hif2a inhibition promotes satellite cell proliferation and muscle regeneration. *J Clin Invest*, 128(6):2339–2355, 2018.
- [74] X. Yang, S. Yang, C. Wang, and S. Kuang. The hypoxia-inducible factors hif1alpha and hif2alpha are dispensable for embryonic muscle development but essential for postnatal muscle regeneration. *J Biol Chem*, 292(14):5981–5991, 2017.
- [75] K. A. Rasbach, R. K. Gupta, J. L. Ruas, J. Wu, E. Naseri, J. L. Estall, and B. M. Spiegelman. Pgc-1alpha regulates a hif2alpha-dependent switch in skeletal muscle fiber types. *Proc Natl Acad Sci U S A*, 107(50):21866–71, 2010.
- [76] L. Wu, H. Yu, Y. Zhao, C. Zhang, J. Wang, X. Yue, Q. Yang, and W. Hu. Hif-2 α mediates hypoxia-induced lif expression in human colorectal cancer cells. *Oncotarget*, 6(6):4406–17, 2015.
- [77] W. Barnard, J. Bower, M. A. Brown, M. Murphy, and L. Austin. Leukemia inhibitory factor (lif) infusion stimulates skeletal muscle regeneration after injury: injured muscle expresses lif mrna. *J Neurol Sci*, 123(1-2):108–13, 1994.
- [78] J. D. White, M. Davies, and M. D. Grounds. Leukaemia inhibitory factor increases myoblast replication and survival and affects extracellular matrix production: combined in vivo and in vitro studies in post-natal skeletal muscle. *Cell Tissue Res*, 306(1):129–41, 2001.
- [79] P. C. Mahon, K. Hirota, and G. L. Semenza. Fih-1: a novel protein that interacts with hif-1alpha and vhl to mediate repression of hif-1 transcriptional activity. *Genes Dev*, 15(20):2675–86, 2001.

- [80] X. Zheng, S. Linke, J. M. Dias, X. Zheng, K. Gradin, T. P. Wallis, B. R. Hamilton, M. Gustafsson, J. L. Ruas, S. Wilkins, R. L. Bilton, K. Brismar, M. L. Whitelaw, T. Pereira, J. J. Gorman, J. Ericson, D. J. Peet, U. Lendahl, and L. Poellinger. Interaction with factor inhibiting hif-1 defines an additional mode of cross-coupling between the notch and hypoxia signaling pathways. *Proc Natl Acad Sci U S A*, 105(9):3368–73, 2008.
- [81] Guglielmo Sorci, Francesca Riuzzi, Cataldo Arcuri, Ileana Giambanco, and Rosario Donato. Amphoterin stimulates myogenesis and counteracts the anti-myogenic factors basic fibroblast growth factor and s100b via rage binding. *Molecular and cellular biology*, 24(11):4880–4894, 2004.
- [82] Y. Li, Y. Liu, Y. Lu, and B. Zhao. Inhibitory effects of 17beta-estradiol or a resveratrol dimer on hypoxia-inducible factor-1alpha in genioglossus myoblasts: Involvement of eralpha and its downstream p38 mapk pathways. *Int J Mol Med*, 40(5):1347–1356, 2017.
- [83] F William Blaisdell. The pathophysiology of skeletal muscle ischemia and the reperfusion syndrome: a review. *Cardiovascular surgery*, 10(6):620–630, 2002.
- [84] M. Belkin, R. D. Brown, J. G. Wright, W. W. LaMorte, and 2nd Hobson, R. W. A new quantitative spectrophotometric assay of ischemia-reperfusion injury in skeletal muscle. *Am J Surg*, 156(2):83–6, 1988.
- [85] Justin J Park, Kirk A Campbell, John J Mercuri, and Nirmal C Tejwani. Updates in the management of orthopedic soft-tissue injuries associated with lower extremity trauma. *Am J Orthop*, 41(02):E27–E35, 2012.
- [86] Thomas M Scalea, Joseph DuBose, Ernest E Moore, Michael West, Frederick A Moore, Robert McIntyre, Christine Cocanour, James Davis, M Gage Ochsner, and David Feliciano. Western trauma association critical decisions in trauma: management of the mangled extremity. *Journal of Trauma and Acute Care Surgery*, 72(1):86–93, 2012.
- [87] Maura H Parker, Patrick Seale, and Michael A Rudnicki. Looking back to the embryo: defining transcriptional networks in adult myogenesis. *Nature Reviews Genetics*, 4(7):497–507, 2003.

- [88] Charlotte A Berkes and Stephen J Tapscott. Myod and the transcriptional control of myogenesis. In *Seminars in cell & developmental biology*, volume 16, pages 585–595. Elsevier, 2005.
- [89] Theodore Kalogeris, Christopher P Baines, Maïke Krenz, and Ronald J Korthuis. Cell biology of ischemia/reperfusion injury. *International review of cell and molecular biology*, 298:229–317, 2012.
- [90] Charles E Murry, Robert B Jennings, and Keith A Reimer. Preconditioning with ischemia: a delay of lethal cell injury in ischemic myocardium. *Circulation*, 74(5): 1124–1136, 1986.
- [91] Chun Y Wong, Hani Al-Salami, and Crispin R Dass. C2c12 cell model: its role in understanding of insulin resistance at the molecular level and pharmaceutical development at the preclinical stage. *Journal of Pharmacy and Pharmacology*, 72(12):1667–1693, 2020.
- [92] R. H. Plasterk. Molecular mechanisms of transposition and its control. *Cell*, 74(5):781–6, 1993.
- [93] R. H. Plasterk, Z. Izsvák, and Z. Ivics. Resident aliens: the tc1/mariner superfamily of transposable elements. *Trends Genet*, 15(8):326–32, 1999.
- [94] Y. Guo, Y. Zhang, and K. Hu. Sleeping beauty transposon integrates into non-ta dinucleotides. *Mob DNA*, 9:8, 2018.
- [95] E. Kowarz, D. Löscher, and R. Marschalek. Optimized sleeping beauty transposons rapidly generate stable transgenic cell lines. *Biotechnol J*, 10(4):647–53, 2015.
- [96] Lajos Mátés, Marinee KL Chuah, Eyayu Belay, Boris Jerchow, Namitha Manoj, Abel Acosta-Sanchez, Dawid P Grzela, Andrea Schmitt, Katja Becker, Janka Matrai, et al. Molecular evolution of a novel hyperactive sleeping beauty transposase enables robust stable gene transfer in vertebrates. *Nature genetics*, 41(6):753–761, 2009.
- [97] Johannes Schindelin, Ignacio Arganda-Carreras, Erwin Frise, Verena Kaynig, Mark Longair, Tobias Pietzsch, Stephan Preibisch, Curtis Rueden, Stephan

- Saalfeld, Benjamin Schmid, et al. Fiji: an open-source platform for biological-image analysis. *Nature methods*, 9(7):676–682, 2012.
- [98] Tamara Pircher, Henning Wackerhage, Elif Akova, Wolfgang Böcker, Attila Aszodi, and Maximilian M Saller. Fusion of normoxic-and hypoxic-preconditioned myoblasts leads to increased hypertrophy. *Cells*, 11(6):1059, 2022.
- [99] J. Y. Li, N. Paragas, R. M. Ned, A. Qiu, M. Viltard, T. Leete, I. R. Drexler, X. Chen, S. Sanna-Cherchi, F. Mohammed, D. Williams, C. S. Lin, K. M. Schmidt-Ott, N. C. Andrews, and J. Barasch. Scara5 is a ferritin receptor mediating non-transferrin iron delivery. *Dev Cell*, 16(1):35–46, 2009.
- [100] M. Kessi, B. Chen, J. Peng, Y. Tang, E. Olatoutou, F. He, L. Yang, and F. Yin. Intellectual disability and potassium channelopathies: A systematic review. *Front Genet*, 11:614, 2020.
- [101] S. C. Chafe, Y. Lou, J. Sceneay, M. Vallejo, M. J. Hamilton, P. C. McDonald, K. L. Bennewith, A. Möller, and S. Dedhar. Carbonic anhydrase ix promotes myeloid-derived suppressor cell mobilization and establishment of a metastatic niche by stimulating g-csf production. *Cancer Res*, 75(6):996–1008, 2015.
- [102] P. Zhao, H. Sharir, A. Kapur, A. Cowan, E. B. Geller, M. W. Adler, H. H. Seltzman, P. H. Reggio, S. Heynen-Genel, M. Sauer, T. D. Chung, Y. Bai, W. Chen, M. G. Caron, L. S. Barak, and M. E. Abood. Targeting of the orphan receptor gpr35 by pamoic acid: a potent activator of extracellular signal-regulated kinase and β -arrestin2 with antinociceptive activity. *Mol Pharmacol*, 78(4):560–8, 2010.
- [103] R. Perniola. Twenty years of aire. *Front Immunol*, 9:98, 2018.
- [104] D. Guidolin, G. Albertin, R. Spinazzi, E. Sorato, A. Mascarini, D. Cavallo, M. Antonello, and D. Ribatti. Adrenomedullin stimulates angiogenic response in cultured human vascular endothelial cells: involvement of the vascular endothelial growth factor receptor 2. *Peptides*, 29(11):2013–23, 2008.
- [105] F. Li, L. Li, X. Qin, W. Pan, F. Feng, F. Chen, B. Zhu, D. Liao, H. Tanowitz, C. Albanese, and L. Chen. Apelin-induced vascular smooth muscle cell proliferation: the regulation of cyclin d1. *Front Biosci*, 13:3786–92, 2008.

- [106] S. M. Nabokina, M. B. Ramos, J. E. Valle, and H. M. Said. Regulation of basal promoter activity of the human thiamine pyrophosphate transporter *slc44a4* in human intestinal epithelial cells. *Am J Physiol Cell Physiol*, 308(9):C750–7, 2015.
- [107] S. Sertic, R. Quadri, F. Lazzaro, and M. Muzi-Falconi. Exo1: A tightly regulated nuclease. *DNA Repair (Amst)*, 93:102929, 2020.
- [108] E. Rigamonti, T. Touvier, E. Clementi, A. A. Manfredi, S. Brunelli, and P. Rovere-Querini. Requirement of inducible nitric oxide synthase for skeletal muscle regeneration after acute damage. *J Immunol*, 190(4):1767–77, 2013.
- [109] M. Gueugneau, D. d’Hose, C. Barbé, M. de Barsy, P. Lause, D. Maiter, L. B. Bindels, N. M. Delzenne, L. Schaeffer, Y. G. Gangloff, C. Chambon, C. Coudy-Gandilhon, D. Béchet, and J. P. Thissen. Increased *serpina3n* release into circulation during glucocorticoid-mediated muscle atrophy. *J Cachexia Sarcopenia Muscle*, 9(5):929–946, 2018.
- [110] K. Sakamoto, Y. Furuichi, M. Yamamoto, M. Takahashi, Y. Akimoto, T. Ishikawa, T. Shimizu, M. Fujimoto, A. Takada-Watanabe, A. Hayashi, Y. Mita, Y. Manabe, N. L. Fujii, R. Ishibashi, Y. Maezawa, C. Betsholtz, K. Yokote, and M. Takemoto. R3hdm1 regulates satellite cell proliferation and differentiation. *EMBO Rep*, 20(11):e47957, 2019.
- [111] F. G. Fowkes, D. Rudan, I. Rudan, V. Aboyans, J. O. Denenberg, M. M. McDermott, P. E. Norman, U. K. Sampson, L. J. Williams, G. A. Mensah, and M. H. Criqui. Comparison of global estimates of prevalence and risk factors for peripheral artery disease in 2000 and 2010: a systematic review and analysis. *Lancet*, 382(9901):1329–40, 2013.
- [112] C. de Theije, F. Costes, R. C. Langen, C. Pison, and H. R. Gosker. Hypoxia and muscle maintenance regulation: implications for chronic respiratory disease. *Curr Opin Clin Nutr Metab Care*, 14(6):548–53, 2011.
- [113] Donna M Mancini, Glenn Walter, Nathaniel Reichek, Robert Lenkinski, Kevin K McCully, James L Mullen, and John R Wilson. Contribution of skeletal muscle atrophy to exercise intolerance and altered muscle metabolism in heart failure. *Circulation*, 85(4):1364–1373, 1992.

- [114] Francesco Saverio Tedesco, Arianna Dellavalle, Jordi Diaz-Manera, Graziella Messina, Giulio Cossu, et al. Repairing skeletal muscle: regenerative potential of skeletal muscle stem cells. *The Journal of clinical investigation*, 120(1): 11–19, 2010.
- [115] E Negroni, GS Butler-Browne, and V Mouly. Myogenic stem cells: regeneration and cell therapy in human skeletal muscle. *Pathologie Biologie*, 54(2):100–108, 2006.
- [116] Satyakam Bhagavati. Stem cell based therapy for skeletal muscle diseases. *Current Stem Cell Research & Therapy*, 3(3):219–228, 2008.
- [117] T. A. Partridge, J. E. Morgan, G. R. Coulton, E. P. Hoffman, and L. M. Kunkel. Conversion of mdx myofibres from dystrophin-negative to -positive by injection of normal myoblasts. *Nature*, 337(6203):176–9, 1989.
- [118] Y. Fan, M. Maley, M. Beilharz, and M. Grounds. Rapid death of injected myoblasts in myoblast transfer therapy. *Muscle Nerve*, 19(7):853–60, 1996.
- [119] D. Skuk, M. Goulet, B. Roy, V. Piette, C. H. Côté, P. Chapdelaine, J. Y. Hogrel, M. Paradis, J. P. Bouchard, M. Sylvain, J. G. Lachance, and J. P. Tremblay. First test of a "high-density injection" protocol for myogenic cell transplantation throughout large volumes of muscles in a duchenne muscular dystrophy patient: eighteen months follow-up. *Neuromuscul Disord*, 17(1):38–46, 2007.
- [120] R. Bischoff. Interaction between satellite cells and skeletal muscle fibers. *Development*, 109(4):943–52, 1990.
- [121] D. Montarras, J. Morgan, C. Collins, F. Relaix, S. Zaffran, A. Cumano, T. Partridge, and M. Buckingham. Direct isolation of satellite cells for skeletal muscle regeneration. *Science*, 309(5743):2064–7, 2005.
- [122] Bide Chen, Wenjing You, Yizhen Wang, and Tizhong Shan. The regulatory role of myomaker and myomixer–myomerger–minion in muscle development and regeneration. *Cellular and Molecular Life Sciences*, 77(8):1551–1569, 2020.

- [123] G_ Cossu, R Kelly, S Di Donna, E Vivarelli, and M Buckingham. Myoblast differentiation during mammalian somitogenesis is dependent upon a community effect. *Proceedings of the National Academy of Sciences*, 92(6):2254–2258, 1995.
- [124] Christine E Holt, P Lemaire, and JB Gurdon. Cadherin-mediated cell interactions are necessary for the activation of myod in xenopus mesoderm. *Proceedings of the National Academy of Sciences*, 91(23):10844–10848, 1994.
- [125] Polina Goichberg and Benjamin Geiger. Direct involvement of n-cadherin-mediated signaling in muscle differentiation. *Molecular biology of the cell*, 9(11): 3119–3131, 1998.
- [126] Julie Gavard, Véronique Marthiens, Céline Monnet, Mireille Lambert, and René Marc Mege. N-cadherin activation substitutes for the cell contact control in cell cycle arrest and myogenic differentiation: involvement of p120 and β -catenin. *Journal of Biological Chemistry*, 279(35):36795–36802, 2004.
- [127] Sophie Charrasse, Mayya Meriane, Franck Comunale, Anne Blangy, and Cé-cile Gauthier-Rouvière. N-cadherin-dependent cell-cell contact regulates rho gtpases and β -catenin localization in mouse c2c12 myoblasts. *The Journal of cell biology*, 158(5):953–965, 2002.
- [128] S. Bensaid, C. Fabre, J. Fourneau, and C. Cieniewski-Bernard. Impact of different methods of induction of cellular hypoxia: focus on protein homeostasis signaling pathways and morphology of c2c12 skeletal muscle cells differentiated into myotubes. *J Physiol Biochem*, 75(3):367–377, 2019.
- [129] Roddy S O'Connor, Craig M Steeds, Robert W Wiseman, and Grace K Pavlath. Phosphocreatine as an energy source for actin cytoskeletal rearrangements during myoblast fusion. *The Journal of physiology*, 586(12):2841–2853, 2008.
- [130] Michael C Hogan, L Bruce Gladden, Bruno Grassi, Creed M Stary, and Michele Samaja. Bioenergetics of contracting skeletal muscle after partial reduction of blood flow. *Journal of Applied Physiology*, 84(6):1882–1888, 1998.
- [131] Naoaki Matsuki, Mutsumi Inaba, and Kenichiro Ono. Catabolism of cytoplasmic and intramitochondrial adenine nucleotides in c2c12 skeletal myotube under chemical hypoxia. *Journal of veterinary medical science*, 64(4):341–347, 2002.

- [132] NA Schroedl, VL Funanage, CR Bacon, SM Smith, and CR Hartzell. Hemin increases aerobic capacity of cultured regenerating skeletal myotubes. *American Journal of Physiology-Cell Physiology*, 255(4):C519–C525, 1988.
- [133] Ahmed Mohyeldin, Tomás Garzón-Muvdi, and Alfredo Quiñones-Hinojosa. Oxygen in stem cell biology: a critical component of the stem cell niche. *Cell stem cell*, 7(2):150–161, 2010.
- [134] Andrea Frudinger, Dieter Kölle, Wolfgang Schwaiger, Johann Pfeifer, Johannes Paede, and Steve Halligan. Muscle-derived cell injection to treat anal incontinence due to obstetric trauma: pilot study with 1 year follow-up. *Gut*, 59(01):55–61, 2010.
- [135] A Frudinger, J Pfeifer, J Paede, V Kolovetsiou-Kreiner, R Marksteiner, and S Halligan. Autologous skeletal-muscle-derived cell injection for anal incontinence due to obstetric trauma: A 5-year follow-up of an initial study of 10 patients. *Colorectal Disease*, 17(9):794–801, 2015.
- [136] Andrea Frudinger, Rainer Marksteiner, Johann Pfeifer, Eva Margreiter, Johannes Paede, and Marco Thurner. Skeletal muscle-derived cell implantation for the treatment of sphincter-related faecal incontinence. *Stem Cell Research & Therapy*, 9(1):1–20, 2018.
- [137] Weixiu Ji, Linjia Wang, Shiyi He, Lu Yan, Tieying Li, Jianxiong Wang, Ah-Ng Tony Kong, Siwang Yu, and Ying Zhang. Effects of acute hypoxia exposure with different durations on activation of nrf2-are pathway in mouse skeletal muscle. *PLoS One*, 13(12):e0208474, 2018.
- [138] Akanksha Agrawal, Richa Rathor, Ravi Kumar, Geetha Suryakumar, and Lilly Ganju. Role of altered proteostasis network in chronic hypobaric hypoxia induced skeletal muscle atrophy. *PLoS One*, 13(9):e0204283, 2018.
- [139] James G Tidball and S Armando Villalta. Regulatory interactions between muscle and the immune system during muscle regeneration. *American Journal of Physiology-Regulatory, Integrative and Comparative Physiology*, 298(5):R1173–R1187, 2010.

- [140] C. L. Mendias, R. Tatsumi, and R. E. Allen. Role of cyclooxygenase-1 and -2 in satellite cell proliferation, differentiation, and fusion. *Muscle Nerve*, 30(4):497–500, 2004.
- [141] K. M. Jansen and G. K. Pavlath. Prostaglandin f2alpha promotes muscle cell survival and growth through upregulation of the inhibitor of apoptosis protein bcl-2. *Cell Death Differ*, 15(10):1619–28, 2008.
- [142] W. Shen, V. Prisk, Y. Li, W. Foster, and J. Huard. Inhibited skeletal muscle healing in cyclooxygenase-2 gene-deficient mice: the role of pge2 and pgf2alpha. *J Appl Physiol (1985)*, 101(4):1215–21, 2006.
- [143] J. F. Markworth and D. Cameron-Smith. Prostaglandin f2 α stimulates pi3k/erk/mTOR signaling and skeletal myotube hypertrophy. *Am J Physiol Cell Physiol*, 300(3):C671–82, 2011.
- [144] D. Blottner and G. Lück. Nitric oxide synthase (nos) in mouse skeletal muscle development and differentiated myoblasts. *Cell Tissue Res*, 292(2):293–302, 1998.
- [145] Natasha C Chang and Michael A Rudnicki. Satellite cells: the architects of skeletal muscle. *Current topics in developmental biology*, 107:161–181, 2014.
- [146] H. Yin, F. Price, and M. A. Rudnicki. Satellite cells and the muscle stem cell niche. *Physiol Rev*, 93(1):23–67, 2013.
- [147] R. W. Ten Broek, S. Grefte, and J. W. Von den Hoff. Regulatory factors and cell populations involved in skeletal muscle regeneration. *J Cell Physiol*, 224(1):7–16, 2010.
- [148] P. L. Puri, S. Iezzi, P. Stiegler, T. T. Chen, R. L. Schiltz, G. E. Muscat, A. Giordano, L. Kedes, J. Y. Wang, and V. Sartorelli. Class i histone deacetylases sequentially interact with myoD and pRB during skeletal myogenesis. *Mol Cell*, 8(4):885–97, 2001.
- [149] J. Hou, L. Wang, H. Long, H. Wu, Q. Wu, T. Zhong, X. Chen, C. Zhou, T. Guo, and T. Wang. Hypoxia preconditioning promotes cardiac stem cell survival and

- cardiogenic differentiation in vitro involving activation of the hif-1 α /apelin/apj axis. *Stem Cell Res Ther*, 8(1):215, 2017.
- [150] Claire Vinel, Laura Lukjanenko, Aurelie Batut, Simon Deleruyelle, Jean-Philippe Pradere, Sophie Le Gonidec, Alizee Dortignac, Nancy Geoffre, Ophelie Pereira, Sonia Karaz, et al. The exerkin apelin reverses age-associated sarcopenia. *Nature medicine*, 24(9):1360–1371, 2018.
- [151] David W Russ and Jane A Kent-Braun. Is skeletal muscle oxidative capacity decreased in old age? *Sports medicine*, 34(4):221–229, 2004.
- [152] Sissel Beate Rønning, Mona Elisabeth Pedersen, Ragnhild Stenberg Berg, Bente Kirkhus, and Rune Rødbotten. Vitamin k2 improves proliferation and migration of bovine skeletal muscle cells in vitro. *PLoS One*, 13(4):e0195432, 2018.
- [153] Shunshun Han, Can Cui, Yan Wang, Haorong He, Zihao Liu, Xiaoxu Shen, Yuqi Chen, Diyan Li, Qing Zhu, and Huadong Yin. Knockdown of csrp3 inhibits differentiation of chicken satellite cells by promoting tgfb β /smad3 signaling. *Gene*, 707:36–43, 2019.
- [154] P. Pomiès, M. Pashmforoush, C. Vegezzi, K. R. Chien, C. Auffray, and M. C. Beckerle. The cytoskeleton-associated pdz-lim protein, alp, acts on serum response factor activity to regulate muscle differentiation. *Mol Biol Cell*, 18(5):1723–33, 2007.
- [155] H. Yin, J. Zhao, H. He, Y. Chen, Y. Wang, D. Li, and Q. Zhu. Gga-mir-3525 targets pdlim3 through the mapk signaling pathway to regulate the proliferation and differentiation of skeletal muscle satellite cells. *Int J Mol Sci*, 21(15), 2020.
- [156] Ming Zheng, Hongqiang Cheng, Indroneal Banerjee, and Ju Chen. Alp/enigma pdz–lim domain proteins in the heart. *Journal of molecular cell biology*, 2(2): 96–102, 2010.
- [157] V. C. Martinelli, W. B. Kyle, S. Kojic, N. Vitulo, Z. Li, A. Belgrano, P. Maiuri, L. Banks, M. Vatta, G. Valle, and G. Faulkner. Zasp interacts with the mechanosensing protein ankrd2 and p53 in the signalling network of striated muscle. *PLoS One*, 9(3):e92259, 2014.

- [158] Stefan G Wette, Heather K Smith, Graham D Lamb, and Robyn M Murphy. Characterization of muscle ankyrin repeat proteins in human skeletal muscle. *American Journal of Physiology-Cell Physiology*, 313(3):C327–C339, 2017.
- [159] Yoshiyuki Tsukamoto, Takao Senda, Toshiya Nakano, Chisato Nakada, Takehiko Hida, Naoko Ishiguro, Gento Kondo, Takeshi Baba, Kenzo Sato, Mitsuhiko Osaki, et al. Arpp, a new homolog of carp, is preferentially expressed in type 1 skeletal muscle fibers and is markedly induced by denervation. *Laboratory investigation*, 82(5):645–655, 2002.
- [160] Melanie K Miller, Marie-Louise Bang, Christian C Witt, Dietmar Labeit, Charles Trombitas, Kaori Watanabe, Henk Granzier, Abigail S McElhinny, Carol C Gregorio, and Siegfried Labeit. The muscle ankyrin repeat proteins: Carp, ankrd2/arpp and darp as a family of titin filament-based stress response molecules. *Journal of molecular biology*, 333(5):951–964, 2003.
- [161] Anja Baumeister, Silvia Arber, and Pico Caroni. Accumulation of muscle ankyrin repeat protein transcript reveals local activation of primary myotube endcompartments during muscle morphogenesis. *The Journal of cell biology*, 139(5):1231–1242, 1997.
- [162] Xin-Hua Liu, William A Bauman, and Christopher Cardozo. Ankrd1 modulates inflammatory responses in c2c12 myoblasts through feedback inhibition of nf- κ b signaling activity. *Biochemical and biophysical research communications*, 464(1):208–213, 2015.
- [163] M. Nishi, A. Mizushima, Ki Nakagawara, and H. Takeshima. Characterization of human junctophilin subtype genes. *Biochem Biophys Res Commun*, 273(3):920–7, 2000.
- [164] P. J. Barton, P. J. Townsend, N. J. Brand, and M. H. Yacoub. Localization of the fast skeletal muscle troponin i gene (tnni2) to 11p15.5: genes for troponin i and t are organized in pairs. *Ann Hum Genet*, 61(Pt 6):519–23, 1997.
- [165] S. Minamisawa, J. Oshikawa, H. Takeshima, M. Hoshijima, Y. Wang, K. R. Chien, Y. Ishikawa, and R. Matsuoka. Junctophilin type 2 is associated with caveolin-3

- and is down-regulated in the hypertrophic and dilated cardiomyopathies. *Biochem Biophys Res Commun*, 325(3):852–6, 2004.
- [166] J. S. Woo, J. H. Hwang, J. K. Ko, N. Weisleder, D. H. Kim, J. Ma, and E. H. Lee. S165f mutation of junctophilin 2 affects ca^{2+} signalling in skeletal muscle. *Biochem J*, 427(1):125–34, 2010.
- [167] J. S. Woo, C. H. Cho, K. J. Lee, D. H. Kim, J. Ma, and E. H. Lee. Hypertrophy in skeletal myotubes induced by junctophilin-2 mutant, y141h, involves an increase in store-operated ca^{2+} entry via orai1. *J Biol Chem*, 287(18):14336–48, 2012.
- [168] N. Toyota and Y. Shimada. Isoform variants of troponin in skeletal and cardiac muscle cells cultured with and without nerves. *Cell*, 33(1):297–304, 1983.
- [169] T. A. Cooper and C. P. Ordahl. A single cardiac troponin t gene generates embryonic and adult isoforms via developmentally regulated alternate splicing. *J Biol Chem*, 260(20):11140–8, 1985.
- [170] Ralph J DeBerardinis and Navdeep S Chandel. Fundamentals of cancer metabolism. *Science advances*, 2(5):e1600200, 2016.
- [171] Sander AJ Verbrugge, Sebastian Gehlert, Lian EM Stadhouders, Daniel Jacko, Thorben Aussieker, Gerard MJ de Wit, Ilse SP Vogel, Carla Offringa, Martin Schönfelder, Richard T Jaspers, et al. Pkm2 determines myofiber hypertrophy in vitro and increases in response to resistance exercise in human skeletal muscle. *International journal of molecular sciences*, 21(19):7062, 2020.
- [172] C. C. Wykoff, N. J. Beasley, P. H. Watson, K. J. Turner, J. Pastorek, A. Sibtain, G. D. Wilson, H. Turley, K. L. Talks, P. H. Maxwell, C. W. Pugh, P. J. Ratcliffe, and A. L. Harris. Hypoxia-inducible expression of tumor-associated carbonic anhydrases. *Cancer Res*, 60(24):7075–83, 2000.
- [173] Andrew J Esbaugh, Steve F Perry, and Kathleen M Gilmour. Hypoxia-inducible carbonic anhydrase ix expression is insufficient to alleviate intracellular metabolic acidosis in the muscle of zebrafish, danio rerio. *American Journal of Physiology-Regulatory, Integrative and Comparative Physiology*, 296(1):R150–R160, 2009.

- [174] J. Huang, D. L. Zheng, F. S. Qin, N. Cheng, H. Chen, B. B. Wan, Y. P. Wang, H. S. Xiao, and Z. G. Han. Genetic and epigenetic silencing of scara5 may contribute to human hepatocellular carcinoma by activating fak signaling. *J Clin Invest*, 120(1):223–41, 2010.
- [175] N. Yan, S. Zhang, Y. Yang, L. Cheng, C. Li, L. Dai, L. Dai, X. Zhang, P. Fan, H. Tian, R. Wang, X. Chen, X. Su, Y. Li, J. Zhang, T. Du, Y. Wei, and H. Deng. Therapeutic upregulation of class a scavenger receptor member 5 inhibits tumor growth and metastasis. *Cancer Sci*, 103(9):1631–9, 2012.
- [176] K. You, F. Su, L. Liu, X. Lv, J. Zhang, Y. Zhang, and B. Liu. Scara5 plays a critical role in the progression and metastasis of breast cancer by inactivating the erk1/2, stat3, and akt signaling pathways. *Mol Cell Biochem*, 435(1-2):47–58, 2017.
- [177] X. Wen, N. Wang, F. Zhang, and C. Dong. Overexpression of scara5 inhibits tumor proliferation and invasion in osteosarcoma via suppression of the fak signaling pathway. *Mol Med Rep*, 13(3):2885–91, 2016.
- [178] Tatu Päätsä. The current understanding of kras protein structure and dynamics. *Computational and structural biotechnology journal*, 18:189–198, 2020.
- [179] Bert Vogelstein and Kenneth W Kinzler. Cancer genes and the pathways they control. *Nature medicine*, 10(8):789–799, 2004.
- [180] H. Kikuchi, M. S. Pino, M. Zeng, S. Shirasawa, and D. C. Chung. Oncogenic kras and braf differentially regulate hypoxia-inducible factor-1alpha and -2alpha in colon cancer. *Cancer Res*, 69(21):8499–506, 2009.

List of Abbreviations

ActRIIb	activin receptor type-2B	7
Adm	adrenomedullin	10
Aire	autoimmune regulator gene	37
AKT	protein kinase B	6
AMPK	AMP-activated protein kinase	7
Ankrd1	Ankyrin repeat doma 1	42
Ankrd2	Ankyrin repeat doma 2	49
Apln	Apelin	38
AR	aspect ratio	18
ATF/CREB	activating transcription factors/ cAMP response element binding protein	4
ATP	adenosine triphosphate	45
BHLHE40	Class E basic helix-loop-helix protein 40	10
CAMKII	calcium/calmodulin-dependent protein kinase II	4
Car9	Carboxy anhydrase 9	37
CASP8AP2	CASP8-associated protein 2	4
CDH2	cadherin 2	44
CDK	cyclin-dependent kinase	5
CDKI	cyclin-dependent kinase inhibitors	5
CDKN1A	cyclin-dependent kinase inhibitor 1A	5
CDKN1B	cyclin-dependent kinase inhibitor 1B	9
CDS	coding sequence	16
COPD	chronisch obstruktive Lungenerkrankung	III
cumPD	cumulative population doubling	19
DAPI	4,6-Diamidine-2-phenylindole dihydrochloride	20

List of Abbreviations

DDIT4	DNA-damage-inducible transcript 4	7
DEG	Differential gene expression	33
DM	differentiation medium	20
DMEM	Dulbecco's Modified Eagle Medium	16
DMSO	dimethyl sulfoxide	18
DR	direct repeats	17
E2	estradiol	12
EDTA	ethylenediaminetetraacetic acid disodium salt dehydrate	16
EPO	erythropoietin	6
ERK1/2	Mitogen-Activated Protein Kinase 3/1	51
FACS	fluorescence-activated cell sorting	17
FBS	fetal bovine serum	16
FBXO32	F-box protein 32	7
FGF	fibroblast growth factor	2
FOXO1	forkhead box O1 transcription factor	4
GFP	green fluorescent protein	16
GM	growth medium	15
Gpr35	G-protein related receptor 35	37
GSEA	gene set enrichment analysis	24
GSK3	glycogen synthase kinase 3 beta	8
H3K27	histone H3 on lysine 27	9
HCA	hierarchical cluster analyses	41
HDAC	histone deacetylase	8
Hes1	hes family bHLH transcription factor 1	4
Hey1	hes related family bHLH transcription factor with YRPW motif 1	4
HEY2	hes related family bHLH transcription factor with YRPW motif 2	4
HGF	hepatocyte growth factor	1
HIF1	Hypoxia-inducible factor 1	10
HIF1A	Hypoxia-inducible factor 1 alpha	10
HIF1AN	hypoxia-inducible factor 1-alpha inhibitor	12
HIF1B	HIF1 beta subunit	10
HIF2A	hypoxia inducible factor 2 alpha	11
HIMGB1	high mobility group protein B1	12

List of Abbreviations

HMOX1	heme oxygenase 1	6
HRE	hypoxia response element	10
HS	horse serum	20
HSP90	heat shock protein 90	10
ID1	inhibitor of differentiation/ DNA binding 1	9
IFA	interferon alpha	35
IFG	interferon gamma	35
IGFII	insulin-like growth factor 2	7
IGFIR	IGFI receptor	7
IL2-STAT5	interleukin 2-signal transducer and activator of transcription 5 . .	35
iNOS	inducible NO synthase	47
IR	inverse repeats	17
JAK2/STAT5a	Janus kinase 2 / signal transducer and activator of transcription 5A	6
JmjC	Jumonji C	10
Jph2	Junctiophilin2	49
Kcna4	Potassium Voltage-Gated Channel Subfamily A Member 4	49
KDM6A	Lysine Demethylase 6A	9
KDM6B	Lysine Demethylase 6B	9
KRAS	Kirsten Rat Sarcoma gene	35
Ldb3	LIM domain binding 3	42
LDH	lactate dehydrogenase	10
Ldlr	Low density lipoprotein receptor gene	48
LFC	log2foldchange	37
LIF	leukemia inhibitor factor	11
MAPK14	mitogen-activated protein kinase family member 14	9
MARP	Muscle ankyrin repeat protein	49
MEF2	myocyte enhancer factor-2	9
miRNA	microRNA	3
MPC	muscle progenitor cell	1
MRF	myogenic regulatory transcription factor	2
MRF4	myogenic regulatory transcription factor 4	9
MRF6	myogenic regulatory transcription factor 6	11
MSTN	myostatin	7

List of Abbreviations

MT	myotubes	1
mTOR1	mammalian target of rapamycin	7
MTORC1	mammalian target of rapamycin complex 1	35
MYH1E	myosin heavy chain 1E	20
Myf5	myogenic factor 5	2
MYF6	myogenic factor 6	6
MYH	myosin heavy chain	3
MYHC1	myosin heavy chain 1	9
MYOD1	myogenic differentiation 1	2
MYOG	myogenin	4
MYOR	myogenic repressor	9
NES	normalized enrichment score	34
NF-kB	nuclear factor kappa-light-chain-enhancer of activated B-cells . .	49
NO	nitric oxide	46
Nos2	nitric oxide synthase 2	39
PAD	peripheral arterial disease	2
PAX3	paired-box transcription factor 3	1
PAX7	paired-box transcription factor 7	1
PBS	phosphate-buffered saline	16
PCA	Principal Component Analysis	24
Pdlim3	Actine-associated LIM protein	42
PDT	population doubling time	19
PFA	paraformaldehyde	20
PFK	phosphofructokinase	10
PG	Prostaglandin	47
PGC-1a	peroxisome proliferator-activated receptor-g coactivator 1a . . .	11
PGF2a	prostaglandin 2 alpha	47
PHD	prolyl hydroxylase	10
PI3K	phosphatidylinositol 3 kinase	6
PK	pyruvate kinase	10
PKC	protein kinase C	4
Ptges3	Prostaglandin E Synthase 3	47
Ptges3l	Prostaglandin Synthase 3 Like	47

List of Abbreviations

Ptgfr	prostaglandin F receptor gene	41
R3hdml	R3h domain containing-like	47
RAGE	receptor for advanced glycation end-products	12
RB	retinoblastoma	5
RFP	red fluorescent protein	16
RHEB	Ras homolog enriched in brain	7
RHOA/JNK	Ras homolog family member A/c-Jun N-terminal kinases	4
ROI	region of interest	18
ROS	reactive oxygen species	3
SB	Sleeping Beauty	16
SC	satellite cell	1
Scara5	Scavenger Receptor Class A Member 5	51
SD	standard deviation	24
SMAD2	SMAD family member 2	7
TNFA	tumor necrosis factor alpha	35
Tnnt2	troponin T2	49
TP53	tumor suppressor p53	5
TRIM63	tripartite motif containing 63	7
TSC	tuberous sclerosis complex	7
VEGF	vascular endothelial growth factor	3
WNT	Wnt signal transduction pathway	V

List of Figures

1.1	Molecular mechanisms involved in self-renewal of satellite cells in hypoxia	5
1.2	Molecular mechanisms involved in myogenic proliferation during hypoxia	8
1.3	HIF1A modulates myogenic differentiation in hypoxia	12
3.1	C2C12 myoblast model	15
3.2	Transfection of fluorescent protein CDS into C2C12 cells by using a SB transposon system	17
3.3	Experiment structur	21
4.1	Morphology and proliferation in hypoxia	26
4.2	Myoblast fusion during hypoxia	27
4.3	Differentiation after transfection of GFP and RFP into C2C12 cells . . .	28
4.4	Fusion of hypoxic with normoxic conditioned myoblasts	30
4.5	Bubble plot of all investigated groups, normalized to N►Diff-N	31
4.6	Analyses of the area, number and size of myotube subpopulations. . . .	33
4.7	PCA and venn diagram	34
4.8	Visualization of the hypoxia dependent hallmarks over the four time points	34
4.9	Heatmap of the 50 most to PC1 or PC2 contributing genes.	36
4.10	Volcano plot of the most differentially regulated genes 24 hours after start of myogenic differentiation.	37
4.11	Volcano plot of the most affected genes after 72 hours	38
4.12	Volcano plot of the most affected genes after 96 hours	39
4.13	Volcano plot of the most affected genes after 144 hours	40
4.14	Hierarchical cluster analysis of the top 50 of 177 genes continuously dif- ferentially regulated genes	41
4.15	Expression and comparison of the 15 selected genes over 144 hours within normoxic and hypoxic conditions	42

List of Tables

3.1	Experimentally evaluated and applied thresholds for each image.	23
-----	---	----

List of Equations

3.1 Cumulative Population Doubling	19
3.2 Mono image creation from three color channels	22

Publications

Systematic Review

Tamara Pircher, Henning Wackerhage, Attila Aszodi, Christian Kammerlander, Wolfgang Böcker and Maximilian Michael Saller, **Hypoxic signaling in skeletal muscle maintenance and regeneration: a systematic review**. *Frontiers in Physiology*, 2021, 12. Jg., S. 684899.

Journal Paper

Pircher Tamara, Wackerhage Henning, Akova Elif, Böcker Wolfgang, Aszodi Attila and Saller Maximilian, **Fusion of Normoxic-and Hypoxic-Preconditioned Myoblasts Leads to Increased Hypertrophy**. *Cells*, 2022, 11. Jg., Nr. 6, S. 1059.



Dekanat Medizinische Fakultät
Promotionsbüro



Eidesstattliche Versicherung

Pircher, Tamara

Name, Vorname

Ich erkläre hiermit an Eides statt, dass ich die vorliegende Dissertation mit dem Titel

Fusion of Normoxic- and Hypoxic-Preconditioned Myoblasts Leads to Increased Hypertrophy

selbständig verfasst, mich außer der angegebenen keiner weiteren Hilfsmittel bedient und alle Erkenntnisse, die aus dem Schrifttum ganz oder annähernd übernommen sind, als solche kenntlich gemacht und nach ihrer Herkunft unter Bezeichnung der Fundstelle einzeln nachgewiesen habe.

Ich erkläre des Weiteren, dass die hier vorgelegte Dissertation nicht in gleicher oder in ähnlicher Form bei einer anderen Stelle zur Erlangung eines akademischen Grades eingereicht wurde.

Egling an der Paar 20.05.2025

Ort, Datum

Pircher Tamara

Unterschrift Tamara Pircher

Acknowledgments

Finally, I want appreciate following people:

Prof. Dr. med. Wolfgang Böcker for beeing my Doktorvater.

Dr. rer. nat. Maximilian Michael Saller for providing me the topic and the access to his lab, for the greatest support during the whole theses and for being the best "Betreuer".

Martina Burggraf for all the technical assistance during my theses, for showing me how to work in a lab and teaching me all the techniques in the lab I needed to learn.

Elif Akova for helping me with the evaluation of the sequencing data.

Prof. Dr. Henning Wackerhage for his experienced scientific ideas and his support during all my publications.

Simon Wölzmüller for all technical support, as well as mental support during the whole theses.

A special thank you to **my family** for their support during my academical studies.

The whole MUM Basic Research Team, for all answered questions during this thesis.



Erklärung zur Übereinstimmung der gebundenen Ausgabe der Dissertation mit der elektronischen Fassung

Pircher, Tamara

Name, Vorname

Hiermit erkläre ich, dass die elektronische Version der eingereichten Dissertation mit dem Titel:

Fusion of Normoxic- and Hypoxic-Preconditioned Myoblasts Leads to Increased Hypertrophy

in Inhalt und Formatierung mit den gedruckten und gebundenen Exemplaren übereinstimmt.

20.05.2025 Egling an der Paar

Ort, Datum

Tamara Pircher

Unterschrift Tamara Pircher